REPORT DOCUMENTATION PAGE

Form Approved OMB NO. 0704-0188

1. REPORT DATE (DD-MM-YYYY)	2. REPORT TYPE	3. DATES COVERED (From - To)
20-08-2015	Book Chapter	-

4. TITLE AND SUBTITLE

Coherent Population Trapping, Nuclear Spin Cooling, and Lévy Flights in Solid-State Atom-Like Systems

5a. CONTRACT NUMBER
W911NF-11-1-0400

5b. GRANT NUMBER

5c. PROGRAM ELEMENT NUMBER
611103

6. AUTHORS
S. Singh, Y. Chu, M. D. Lukin, S. F. Yelin

5d. PROJECT NUMBER

5e. TASK NUMBER

5f. WORK UNIT NUMBER

7. PERFORMING ORGANIZATION NAMES AND ADDRESSES
Massachusetts Institute of Technology (MIT
77 Massachusetts Ave.
NE18-901
Cambridge, MA 02139 -4307

8. PERFORMING ORGANIZATION REPORT NUMBER

9. SPONSORING/MONITORING AGENCY NAME(S) AND ADDRESS (ES)

U.S. Army Research Office
P.O. Box 12211
Research Triangle Park, NC 27709-2211

10. SPONSOR/MONITOR'S ACRONYM(S)
ARO

11. SPONSOR/MONITOR'S REPORT NUMBER(S)
59745-PH-MUR.149

12. DISTRIBUTION AVAILIBILITY STATEMENT

Approved for public release; distribution is unlimited.

13. SUPPLEMENTARY NOTES

The views, opinions and/or findings contained in this report are those of the author(s) and should not contrued as an official Department of the Army position, policy or decision, unless so designated by other documentation.

14. ABSTRACT

We describe and analyze a method for controlling nuclear spin environment of atom-like quantum emitters in the solid state. The method makes use of laser manipulation of an electronic spin transition via coherent population trapping. Specifically, we present a detailed description of the nuclear spin dynamics and its interplay with the optical exci-tation of the electronic spin of nitrogen-vacancy color centers in diamond. We intro-duce a simple model of this process that allows us to study both optimal cooling parameters for nuclear spins and optimal ....

15. SUBJECT TERMS

Quantum, Nuclear spin

16. SECURITY CLASSIFICATION OF:			17. LIMITATION OF ABSTRACT	15. NUMBER OF PAGES	19a. NAME OF RESPONSIBLE PERSON
a. REPORT	b. ABSTRACT	c. THIS PAGE			Paola Cappellaro
UU	UU	UU	UU		19b. TELEPHONE NUMBER 617-253-8137

Report Title

Chapter Eleven - Coherent Population Trapping, Nuclear Spin Cooling, and Lévy Flights in Solid-State Atom-Like Systems

ABSTRACT

We describe and analyze a method for controlling nuclear spin environment of atom-like quantum emitters in the solid state. The method makes use of laser manipulation of an electronic spin transition via coherent population trapping. Specifically, we present a detailed description of the nuclear spin dynamics and its interplay with the optical exci-tation of the electronic spin of nitrogen-vacancy color centers in diamond. We intro-duce a simple model of this process that allows us to study both optimal cooling parameters for nuclear spins and optimal information transfer between the optical mea-surement of the electron and the nuclear bath dynamics. This allows us to investigate the statistical properties of the nuclear spin bath. Potential applications to quantum information processing and quantum metrology are possible.

CHAPTER ELEVEN

Coherent Population Trapping, Nuclear Spin Cooling, and Lévy Flights in Solid-State Atom-Like Systems

Swati Singh[*,†], Yiwen Chu[‡], Mikhail Lukin[§], Susanne Yelin[†,§,1]
[*]ITAMP, Harvard-Smithsonian Center for Astrophysics, Cambridge, Massachusetts, USA
[†]Department of Physics, University of Connecticut, Storrs, Connecticut, USA
[‡]Department of Applied Physics, Yale University, New Haven, Connecticut, USA
[§]Department of Physics, Harvard University, Cambridge, Massachusetts, USA
[1]Corresponding author: e-mail address: syelin@physics.harvard.edu

Contents

Advances in Atomic, Molecular, and Optical Physics, Volume 64
ISSN 1049-250X
http://dx.doi.org/10.1016/bs.aamop.2015.05.001

Abstract

We describe and analyze a method for controlling nuclear spin environment of atom-like quantum emitters in the solid state. The method makes use of laser manipulation of an electronic spin transition via coherent population trapping. Specifically, we present a detailed description of the nuclear spin dynamics and its interplay with the optical excitation of the electronic spin of nitrogen-vacancy color centers in diamond. We introduce a simple model of this process that allows us to study both optimal cooling parameters for nuclear spins and optimal information transfer between the optical measurement of the electron and the nuclear bath dynamics. This allows us to investigate the statistical properties of the nuclear spin bath. Potential applications to quantum information processing and quantum metrology are possible.

1. INTRODUCTION

Intense recent interest in solid-state quantum emitters is being driven by their unique potential applications to nanoscale sensors (Balasubramanian et al., 2008; Kucsko et al., 2013; Maletinsky et al., 2012; Maze et al., 2008; Sage et al., 2013) and realization of novel quantum information platforms (Bernien et al., 2013; Neumann et al., 2008). These atom-like solid-state defects combine the tunability and precision of atomic systems, along with the robust and scalable infrastructure provided by solid-state devices (Weber et al., 2010). Many defects in solid-state materials, such as quantum dots in semiconductors (Hennessy et al., 2007) and color centers in diamond (Wrachtrup and Jelezko, 2006) or silicon (Baranov et al., 2011) have emerged as competitive platforms for such quantum based technologies. However, the practical performance of these systems is limited by strong interactions of solid-state defects with their local environment. For example, the electronic spin coherence properties of atom-like systems are limited by the random Overhauser field, which is the effective field created by the interaction of the random surrounding nuclear spins (Awschalom et al., 2013). It originates due to the interaction of the electron spin with the surrounding nuclear spins consisting of both Fermi contact and dipole–dipole interactions, which cannot be turned off entirely using dynamical decoupling techniques.

The goal of *nuclear spin cooling* is to eliminate or considerably suppress the electronic spin decoherence due to surrounding nuclei. Within this context, nuclear spin cooling can take place when one or several electron

spins, polarized and controlled by fine-tuned lasers and other external fields, interact with *all* surrounding nuclear spins. This can amount to about 10^4–10^5 nuclear spins of all the surrounding atoms in typical semiconductor quantum dots or to as few as the 10–100 spins of the ^{13}C atoms in an otherwise spinless ^{12}C diamond lattice. The quantum dynamics of a solid-state defect center can be described by a central spin model, in which the (central) electron spin can be controlled directly, while the environment of nuclear spins is only indirectly accessible via the electron (Prokof'ev and Stamp, 2000). The spin interactions existing in this system encompass three distinct time scales: (i) the interaction of the electron spin with electromagnetic fields, in the range of 1–100 MHz; (ii) the hyperfine and dipole–dipole interaction between electron and nuclear spins (of the order of 0.01–10s of MHz), which are responsible for the Overhauser field; and (iii) the dipole–dipole interaction among the nuclear spins, of the order of mostly a few kHz. One specific approach involves the optical technique known as "coherent population trapping" (CPT). The essence of this techniques, widely known in atomic systems, is that the atomic population is trapped in a superposition of electronic states, decoupled from the laser fields, known as the "dark state." Over the past two decades, CPT has been employed for laser cooling of neutral atoms (Aspect et al., 1988) and ions (Roos et al., 2000), creation of ultra-cold molecules (Ni et al., 2008), optical magnetometry (Budker and Romalis, 2007; Scully and Fleischhauer, 1992), and atomic clocks (Vanier, 2005), as well as for slowing and stopping light pulses (Fleischhauer et al., 2005). The same technique has been applied to solid-state systems including the nitrogen-vacancy (NV) center in diamond (Santori et al., 2006), and individual quantum dots (Xu et al., 2009) where interesting dynamics between the quantum dot and its nuclear environment have been observed. In particular, this quantum optical technique can be used for cooling, measurement and manipulation of artificial atom-like solid-state systems and their local environment (Giedke et al., 2006; Issler et al., 2010; Stepanenko et al., 2006; Xu et al., 2009).

Specifically, the method can be applied to cooling, real-time projective measurement and control of the nuclear spin environment surrounding the electronic spin qubit associated with individual NV centers in diamond (Batalov et al., 2009; Hanson et al., 2006). The NV center has a long-lived spin triplet as its electronic ground state (Manson et al., 2006), whose $m_s = \pm 1, 0$ sublevels are denoted as $|\pm 1\rangle$ and $|0\rangle$ in the following. In pure

samples, the electron spin dynamics are governed by interactions with the spin-1 ^{14}N nucleus of the NV center and spin-1/2 ^{13}C nuclei present in 1.1% natural abundance in the diamond lattice (Fig. 1a). Control over nuclear spins (Dutt et al., 2007; Neumann et al., 2010) is of interest for both fundamental studies and for applications such as nanoscale magnetic sensing (Balasubramanian et al., 2008; Maze et al., 2008) and realization of quantum networks (Childress et al., 2006; Togan et al., 2010).

In a recent experimental study, such control was achieved via two complimentary methods: effective cooling of nuclear spins through nuclear state selective CPT (Issler et al., 2010) and conditional preparation based on fast

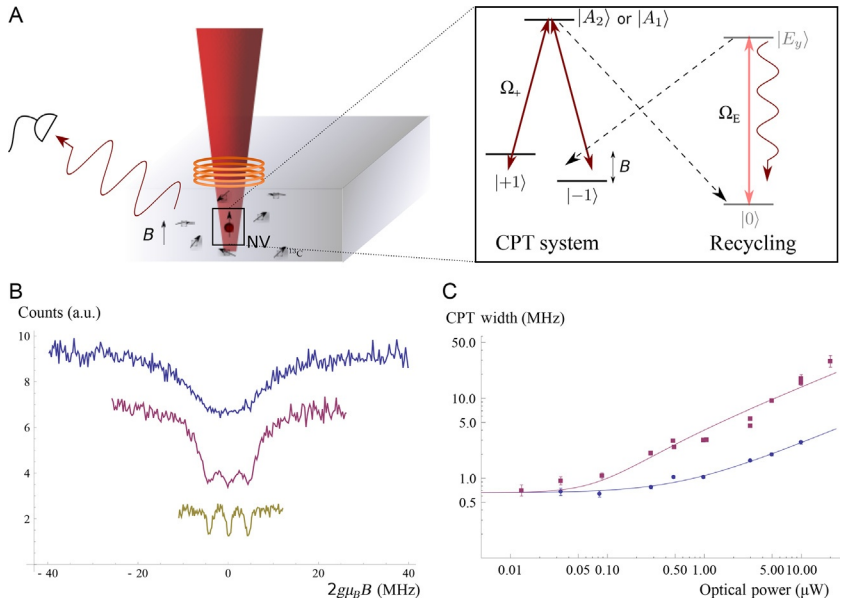

Figure 1 Coherent population trapping in NV centers. (a) The Λ-type transitions between the ground states $|\pm 1\rangle$ and excited states $|A_{1,2}\rangle$ of a single NV center are addressed with a CPT laser (Rabi frequency Ω_+),while a recycling laser (Rabi frequency Ω_E) drives the $|0\rangle$ to $|E_y\rangle$ transition. An external magnetic field B is applied using a solenoid, producing a ground state splitting $2g\mu_B B$. (b) Photon counts from the NV in a 300-μs window are plotted versus the applied field for 10 μW (blue (black in the print version), upper), 3 μW (red (dark gray in the print version), middle), and 0.1 μW (yellow (gray in the print version), lower) of laser power addressing the $|A_2\rangle$ state. Blue (black in the print version) and red (dark gray in the print version) datasets are shifted vertically by 5 and 2 counts for clarity. (c) Width of individual ^{14}N CPT lines versus CPT laser power when the $|A_1\rangle$ (blue (dark gray in the print version), lower) or $|A_2\rangle$ (red (gray in the print version), upper) state is used. Error bars in all figures show $\pm$ 1 s.d. Solid curves represent theoretical models. *Figure reprinted with permission from Togan et al. (2011).*

measurements of the nuclear environment and subsequent postselection (Giedke et al., 2006). While most prior work involved the use of microwave and RF fields for manipulating both the electronic and nuclear spin states, in the experiments of Togan and coworkers all-optical control of the electronic spin (Buckley et al., 2010; Robledo et al., 2010; Santori et al., 2006; Togan et al., 2011) was utilized.

The goal of this article is to review this method and to analyze the following questions: How can optical techniques be used to optimally cool a nuclear spin bath? What are the specifics of the laser cooling/CPT process in diamond NV centers? How can we model the nuclear spin dynamics in such a system? In particular, this raises the additional question as to how this spin cooling method compares to some of the above-mentioned CPT techniques in atomic and quantum dot systems. And which parameter regions are most interesting for cooling or "freezing"[1] the nuclear spin environment and which ones, in contrast, are optimal for measuring statistics of the nuclear spin dynamics?

In what follows, after a short exposé of the experimental results, we introduce a generic model for a central spin systems with different electronic and nuclear spin interactions, we explain in detail the mechanisms for nuclear spin cooling using CPT, both in general and for NV centers in particular. We introduce a random walk model that allows us to understand how to manipulate nuclear dynamics and helps to choose the best cooling conditions and the cleanest examples for unusual statistics such as Lévy flights.

2. PHYSICAL SYSTEM AND EXPERIMENTS: OVERVIEW

In this section, we review recent experiments that use the NV center's optical transitions and coherent population trapping (CPT) to manipulate its surrounding spin bath and describe in more detail the physical system: the spin of the ^{14}N nucleus associated with the NV center itself and the ^{13}C nuclei in the diamond lattice (see Childress et al., 2014; Chu and Lukin, 2014 for recent reviews), then describe the mechanics of the system.

[1] We use here the distinction between *freezing* as trapping the spins in one single state and *cooling* as narrowing down considerably the energy distribution of the trapped spin states without necessarily narrowing down to one single state only.

Specifically, one makes use of Λ-type level configurations involving the NV center's $|A_1\rangle$ and $|A_2\rangle$ optically excited electronic states and the $|\pm 1\rangle$ ground states (Fig. 1a) (Maze et al., 2011; Togan et al., 2010). At low temperatures (<10 K) and in the limit of zero strain, $|A_1\rangle$ and $|A_2\rangle$ are entangled states of spin and orbital momentum coupled to the $|+1\rangle$ ($|-1\rangle$) state with σ_- ($\sigma+$) circularly polarized light. Correspondingly, excitation with linearly polarized light drives the NV center into a so-called dark superposition state when the two-photon detuning is zero (Scully and Zubairy, 1997). In the present case the two-photon detuning is determined by the Zeeman splitting between the $|\pm 1\rangle$ states due to the combined effect of the Overhauser field originating from the nuclear spin environment and any externally applied magnetic field (Issler et al., 2010; Stepanenko et al., 2006). When the external field exactly compensates the Overhauser field, the electronic spin of the NV center is pumped into the dark state after a few optical cycles and remains in the dark state, resulting in vanishing fluorescence. This is the essence of the dark resonances and CPT.

2.1 Coherent Population Trapping with NV Centers

In the experiments, the $|A_1\rangle$ and $|A_2\rangle$ states are separated by approximately 3 GHz and are addressed individually with a single linearly polarized laser at near zero magnetic field. Since there is a finite branching ratio from the $m_s = \pm 1$ manifold of the electron spin into the $|0\rangle$ state, a recycling laser is used that drives the transition between $|0\rangle$ and the $|E_y\rangle$ excited state, which decays with a small but nonvanishing probability ($\sim 10^{-2}$) back to the $|\pm 1\rangle$ states. Figure 1b presents experimental observation of the CPT spectrum as a function of an external magnetic field at three different powers of a laser tuned to the $|\pm 1\rangle \rightarrow |A_2\rangle$ transition. While a broad resonance is observed at high power levels, as the power is reduced, we clearly resolve three features in the spectrum separated by 4.4 MHz, which is 2× the hyperfine splitting between three ^{14}N nuclear spin states. This separation corresponds to the magnetic field required to bring the electronic $m_s = \pm 1$ hyperfine states with equal nuclear spin projection ($m_I = \pm 1, 0$) of the spin-1 ^{14}N nucleus of the NV center into two-photon resonance.

The dependence of the CPT resonance width upon the laser power, shown in Fig. 1c, reveals the important role played by repumping on the near-cycling $|0\rangle \leftrightarrow |E_y\rangle$ transition. In contrast to a conventional, closed three-level system, this recycling transition can be used to enhance the utility of our CPT system by both decreasing the width of the CPT resonance and

increasing the signal to noise ratio. The $|A_1\rangle$ state decays into the $m_s = 0$ ground state through the singlet with a substantial probability of $\sim 40\%$. However, the population is returned back into the $m_s = \pm 1$ state from $|E_y\rangle$ only after ~ 100 optical excitation cycles. As a result, away from the two-photon resonance, the NV quickly decays to the $|0\rangle$ state after being excited, where it then scatters many photons through the $|0\rangle \leftrightarrow |E_y\rangle$ cycling transition before returning to the Λ system. If the NV center is not in a dark state, this process effectively increases the number of photons we collect by γ_{s1}/γ_{ce}, where γ_{ce} is the cross transition rate from $|E_y\rangle$ into $|\pm 1\rangle$ and γ_{s1} is the rate from $|A_1\rangle$ to the singlet. The cycling effect also reduces the width of the CPT line since the $|0\rangle \leftrightarrow |E_y\rangle$ transition is quickly saturated away from two-photon resonance, provided that the CPT laser excitation rate exceeds the leakage rate out of recycling transition. Significantly, both of these effects lead to improved sensitivity of dark resonances to small changes in two-photon detuning.

To demonstrate this effect, the widths of dark resonances observed via excitation of $|A_1\rangle$ and $|A_2\rangle$ are compared in Fig. 1c. The experimental results of an independent measurement of the respective branching ratios are compared with a simple theoretical model described in Togan et al. (2011). The width at low powers is determined by the random magnetic field associated with surrounding ^{13}C nuclear states. When this line broadening mechanism is taken into account, the experimental results are in excellent agreement with the theoretical predictions, plotted as solid lines, showing that a high degree of optical control over the electronic spins of NV center can be achieved.

Subsequent experiments using the NV interaction with the spin-1/2 ^{13}C nuclei (Togan et al., 2011) showed that CPT can be used for not only probing the nuclear spin environment of the NV center, but also controlling and preparing the state of the spin bath. For the ^{14}N spins, it is possible to optically cool the nuclear spin states using dark resonances. The physics is reminiscent of laser cooling of atomic motion via velocity-selective CPT (Aspect et al., 1988; Issler et al., 2010). A redistribution of the ^{14}N spin state population upon optical excitation takes place because the hyperfine coupling in the excited electronic state of the NV center is enhanced by a factor of ~ 20 compared to the ground state (Fuchs et al., 2008). If the external field is set such that, for example, the $m_I = 0$ hyperfine states are in a dark state owing to the two-photon resonance, only the states with nuclear configuration $m_I = \pm 1$ will be promoted to the excited states. In this excited state,

flip-flops with the electron spin will change the nuclear spin to the $m_I = 0$ states. When the NV center spontaneously decays into the dark superposition of electronic spin states, optical excitation will cease, resulting in effective polarization (cooling) of nuclear spin into $m_I = 0$ state.

This technique can also be extended to control the many-body environment of the NV center, consisting of ^{13}C nuclei distributed throughout the diamond lattice. The large number of nuclear spin configurations associated with an unpolarized environment results in a random Overhauser field (B_{OF}) with unresolved hyperfine lines. It produces a finite CPT linewidth in measurements that average over all configurations of the ^{13}C spin bath (Fig. 1b and c). However, one can make use of fast measurements and the long correlation time (T_1^{nuc}) associated with evolution of the nuclear bath to observe its instantaneous state and manipulate its dynamics. For example, such a fast measurement is illustrated in Fig. 2a, where the B externally applied field is ramped across a single ^{14}N $m_I = 0$ line while the CPT lasers are on, and the counts collected in 80 μs time bins are plotted for successive individual runs, many of which distinctly show a narrow dark region. Lorentzian fits to selected experimental scans reveal "instantaneous" CPT resonances with linewidths that are over a factor three less than those of the averaged measurement. The motion of the dark line centers (green (gray in the print version) dots in Fig. 2a) indicates that the instantaneous field evolves in time. Fast measurements can also be used to conditionally prepare the ^{13}C environment of the NV center in a desired state with postselection. Here, the nuclear spins are first prepared though optical excitation at a fixed value of the external magnetic field B_{prep}, as shown in Fig. 2b. By conditionally selecting zero photon detection events during this preparation step, we can select the states of the ^{13}C environment with vanishing two-photon detuning $\delta = 2g\mu_B(B_{\mathrm{prep}} + B_{\mathrm{OF}}) = 0$, where μ_B is the Bohr magneton. The resulting modified distribution of Overhauser field is then probed in a readout step by rapidly the changing magnetic field value to B_{RO}, which is scanned across the resonance. The middle curve in Fig. 2c shows (unconditioned) readout counts recorded following the preparation step, while the bottom curve shows the result of measurement-based preparation. The measured width of such a conditionally prepared distribution is significantly smaller than the width corresponding to individual ^{14}N resonances obtained without preparation. In what follows we present a detailed theoretical description of these physical phenomena.

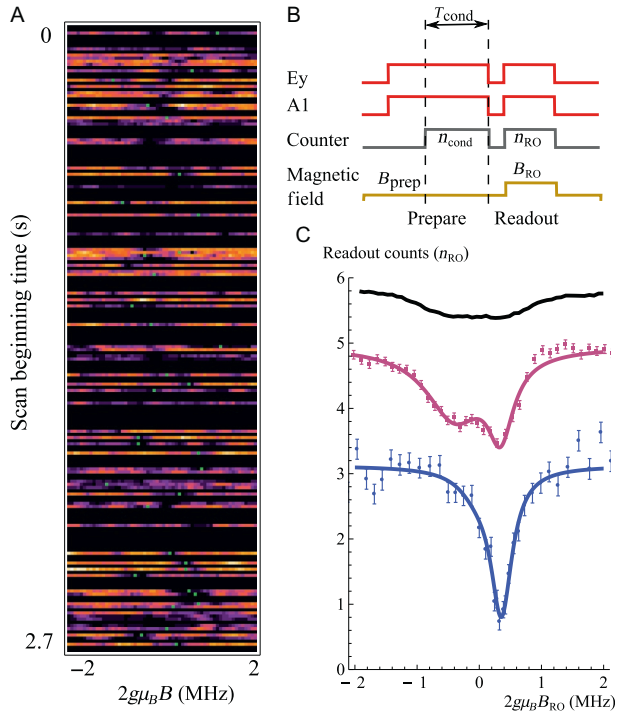

Figure 2 Fast measurement and preparation of ^{13}C spin bath. (a) Counts from 200 successive fast magnetic field ramps are shown on horizontal lines. The centers of Lorentzian fits to individual runs are indicated with a green (gray in the print version) dot. (b) Pulse sequence for preparation and subsequent measurement of the ^{13}C configuration. The preparation magnetic field B_{prep} is set within the central ^{14}N line while the readout field B_{RO} is varied to cover all associated ^{13}C states. The n_{cond} counts during a conditioning window of length T_{cond} at the end of preparation and the n_{RO} counts during the readout window are recorded for each run. Data presented is an average of many such experimental runs. (c) n_{RO} versus B_{RO} is shown in the middle plot with double Lorentzian fit. The same dataset analyzed by keeping only events with $n_{cond} = 0$ is shown in the bottom plot. Unprepared ^{13}C distribution is shown in the top plot for comparison (shifted by 4.3 counts for clarity). *Figure reprinted with permission from Togan et al. (2011).*

2.2 Model: Laser–NV Interaction

The general Hamiltonian for electronic and nuclear spins in the presence of an external magnetic field is

$$H = H_{opt} + H_{NV} + H_{bath} + H_{int}. \quad (1)$$

Here, H_{opt} describes the interaction of the NV with the optical fields, $H_{NV} = \hbar\Delta S_z^2 - \hbar\mu_e \mathbf{S}.\mathbf{B}$, where $\Delta/2\pi = 2.87$ GHz, the zero-field splitting of the NV and the latter term describes the electronic Zeeman shift. Since Δ is the dominant energy scale, the $|\pm 1\rangle$ energy levels are significantly higher in energy than the $|0\rangle$ state, as shown in Fig. 1a. The nuclear Hamiltonian (H_{bath}) consists of the nuclear Zeeman and dipole–dipole interaction, and H_{int} describes the hyperfine interaction between the ^{13}C bath and the electronic spin of the NV center.

Three different timescales dominate the dynamics of the system. The fastest timescale is given by the optical excitation of the NV electronic spin. We model it as a five-level atomic system coupled to two lasers. The goal is to pump the spin into an electronic dark state with respect to the laser fields via coherent population trapping. The second fastest timescale in the coupled system is given by the hyperfine interaction between the NV state and the ^{13}C nuclear spin bath. This hyperfine coupling leads to splitting of the electronic spin states, and thus the two-photon resonance condition is ideally only satisfied for a particular nuclear spin configuration (or a small subset of available configurations). Thus, we end up optically pumping the NV in a dark state corresponding to a particular nuclear spin configuration, which we call $|D_{\text{nuc}}\rangle$. The slowest interaction in the system is the interaction between the ^{13}C nuclei forming the spin bath of the NV, which is suppressed for state $|D\rangle$ due to the other two interactions. While the two faster processes lead to trapping in a dark state, this very slow dynamics destroy the trapped state, and thus determine the ultimate limit of the nuclear spin cooling potential of this scheme. In the following, we discuss each H_{opt}, H_{bath} and H_{int} separately and how it affects nuclear spin diffusion.

After making the rotating wave approximation, the Hamiltonian for laser–NV interaction is given by

$$H_{\text{opt}} = -\hbar/2\left(\Omega_+ |B\rangle\langle A_1| + \delta|D\rangle\langle B| + \Omega_E|0\rangle\langle E_y| + \text{c.c.}\right). \tag{2}$$

The laser field couples the A_1 state to the bright state $|B\rangle = (|+1\rangle + |-1\rangle)/\sqrt{2}$ with a Rabi frequency of $\Omega_+ = \sqrt{2} \times \Omega_1$. On the other hand, the dark state $|D\rangle = (|+1\rangle - |-1\rangle)/\sqrt{2}$ is decoupled from the laser field. Here, δ corresponds to the two-photon detuning between the $|\pm 1\rangle$ states due to interaction with external magnetic fields (B_{ext}) and nuclear spin bath (B_{OF}), the details of which will be considered later. Since the nuclear

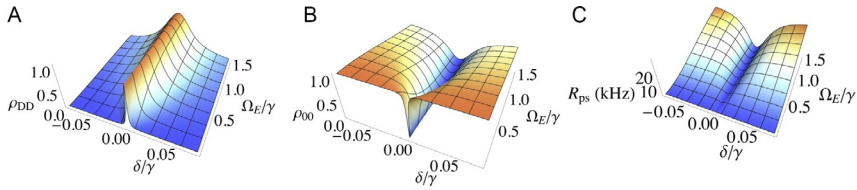

Figure 3 Steady state populations in ground states $|D\rangle$ (a) and $|0\rangle$ (b) as a function of detuning and Ω_E repumping laser Rabi frequency. Rabi frequency $\Omega_+ = \sqrt{2} \times 0.8\gamma$. (c) **Calculated photon scattering rate R_{ps}** from the excited state, **defined in Eq. (A.8) of Appendix A**, as a function of same parameters for a collection efficiency $\eta = 10^{-2}$.

spin bath dynamics occurs on much longer timescales than the ones associated with laser–NV interaction, we assume that the NV adiabatically follows the random changes in δ due to bath dynamics.

In this analysis, the Liouvillian takes into account spontaneous emission and dephasing. Since we are interested in the long-time behavior of the system ($t \gg 1/\gamma$), we assume that the system (NV spin interacting with lasers) has evolved into a steady state. The details of the calculation of steady state is given in Appendix A. Figure 3 shows the steady state population in the electronic ground states as a function of detuning δ.

We observe from Fig. 3 that the NV is primarily in the dark state $|D\rangle$ or in state $|0\rangle$. At resonance ($\delta = 0$), the NV is in the dark state, and for large detuning, the NV is most likely in $|0\rangle$, where there is no hyperfine interaction. This division of population is an important condition for CPT based nuclear spin cooling scheme that we discuss in detail later.

2.3 Hyperfine Interaction

The Hamiltonian for an NV interacting with its bath gives a more specific form of the Hamiltonian given in Eq. (1):

$$H = H_{\text{opt}} + H_{\text{bath}} + \hbar\Delta S_z^2 - \hbar\mu_e \mathbf{S}.\mathbf{B} + \hbar \sum_{j,\mu,\nu} S_\mu A^j_{\mu\nu} I^j_\nu, \tag{3}$$

where H_{bath} will be discussed later, and the other terms are the zero-field splitting, electronic Zeeman interaction and hyperfine interaction respectively. Here, μ,ν denote the x,y,z spin of the j-th nuclear spin. There are two types of hyperfine interaction in central spin systems: the isotropic Fermi contact interaction, and the dipole–dipole interaction. The former is dominant if the electronic and nuclear wave functions overlap sufficiently,

as in the case of quantum dots and other shallow donors (Zhao et al., 2012). For an NV^- spin coupled to ^{13}C nuclei beyond the first few coordinate shells, the dipolar interaction is dominant, leading to an anisotropic hyperfine interaction (Hall et al., 2014; Mizuochi et al., 2009).

To understand the primary role of hyperfine interaction in this CPT cooling scheme, we start with a simple system of an NV spin coupled to a single spin 1/2 system, corresponding to a ^{13}C spin. For this treatment, we briefly move to the $|\pm 1\rangle, |0\rangle$ electronic ground state basis of Section 2.1. For clarity, we define a detuning operator $\delta_\mu = \sum_\nu A_{\mu\nu} I_\nu - \mu_e B_\mu$, where the form of $A_{\mu\nu}$ is discussed in detail in Appendix B. With these definitions, the Hamiltonian from Eqs. (1) and (3) can be written as

$$H = H_{\text{opt}} + H_{\text{bath}} + \hbar\Delta S_z^2 + \hbar S_z \delta_z + \hbar S_x \delta_x + \hbar S_y \delta_y. \tag{4}$$

Due to the disparity between the dipole moments of electronic and nuclear spins ($\mu_e \sim 2000\mu_n$), nuclear-electronic spin flip-flop interactions (corresponding to $S_\pm I_\mp$) are highly nonresonant. Furthermore, due to the presence of a large zero-field splitting (Δ) in NV centers, all terms with $S_\pm$ are highly suppressed.[2] Therefore, hyperfine interaction does not lead to any spin flip-flops between the electronic and nuclear spins. Assuming a large magnetic field, the terms with $S_z I_\pm$ are also suppressed due to the nuclear Zeeman energy cost of these transitions. Approximating $H_{\text{int}} \approx \hbar A_z S_z I_z$, we find that it leads to a split in the ± 1 ground state spin manifold, depending on the two orientations of the nuclear spin, as illustrated in Fig. 4a. Due to this splitting in the ± 1 manifold, the two-photon resonance condition is no longer satisfied. This splitting can be thought of as due to an effective B-field that the NV spin experiences due to the orientation of nuclear spin. This nuclear spin state dependent effective B-field represents the Overhauser field mentioned in the previous section. However, one could shift the ± 1 ground states with respect to each other by applying an external field, as illustrated in Fig. 4b. The nuclear spin does not interact strongly with this field due to its considerably smaller gyromagnetic ratio.

An important observation here is that there exists an external field that cancels the effect of the hyperfine interaction-induced shift for a particular nuclear spin orientation. By applying appropriately intense laser fields, one

[2] As a second order effect, this interaction leads to an enhanced gyromagnetic ratio and hyperfine mediated nuclear spin–spin interaction as discussed in Appendix B.

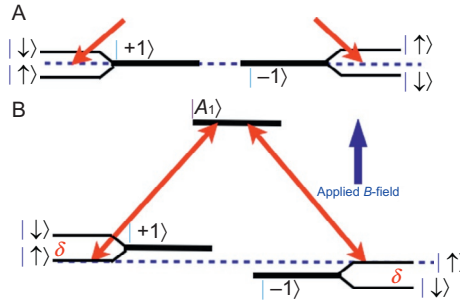

Figure 4 Level diagram of the energy levels involved in the electronic Λ system coupled to a single spin 1/2 via hyperfine interaction. (A) The presence of another spin splits the +/−1 energy levels. (B) An external field shifts these manifolds with respect to each other, bringing the levels corresponding to a particular nuclear spin configuration (here $|\uparrow\rangle$) in two-photon resonance with the CPT lasers.

can create a dark state of the electronic spin corresponding to only one particular nuclear spin configuration—thus using a combined electronic and nuclear dark state in which to optically pump. Thus, after several spontaneous emission events, the system relaxes into this trapped state.

For the case of multiple nuclear spins, we define a new detuning operator,

$$\delta_z = \sum_j A^j_{zz} I^j_z - \mu_e B_z, \tag{5}$$

that sums over the hyperfine interaction of all the bath nuclear spins. This coupling does not lead to any quantitative changes in our understanding, except that now the electronic ground states are split into the 2^N states of N nuclear spins. Appendix C simulates the hyperfine coupling distribution of a realistic ^{13}C nuclear spin ensemble in a diamond lattice. In spite of having a large number of energy levels, very few nuclear spin configurations (in principle only one) satisfy the two-photon resonance condition. With the change of basis to $|B\rangle$, $|D\rangle$, we can rewrite the Hamiltonian given in Eq. (3) as

$$H = H_{\text{bath}} + \hbar\Delta S_z^2 + \hbar\delta_z(|D\rangle\langle B| + |B\rangle\langle D|). \tag{6}$$

Equation (6) clearly shows how the hyperfine interaction leads to transitions between $|B\rangle$ and $|D\rangle$ states. In fact, the detuning δ in CPT analysis in the previous section is equal to "detuning" δ_z from the resonant nuclear spin configuration. From now on, we shall label this detuning due to the difference between external and Overhauser field as δ. This type of CPT based

cooling of the nuclear spin was demonstrated in the case of NVs (Togan et al., 2011), and optically addressable quantum dots (Xu et al., 2009).

For small magnetic fields, the $S_z I_\pm$ cannot be ignored, and is the prominent cause of change in the Overhauser field (Dréau et al., 2014). However, as discussed previously, due to interaction with laser fields, the NV electronic spin is pumped into $|0\rangle$ or $|D\rangle$, both of them having $\langle S_z \rangle = 0$. Hence the hyperfine interaction does not directly cause nuclear spin flips, even for small magnetic fields. We now investigate interactions in the spin bath itself.

2.4 Nuclear Bath Dynamics

An important distinction between most systems coupled to a Markovian bath and the spin bath of a central spin is that the bath dynamics cannot be ignored. Along with giving the fundamental line width to the 2^N energy levels discussed in the previous section, the bath dynamics leads to changes in the nuclear spin configuration.

The dominant interactions in the nuclear bath are their nuclear Zeeman, dipole–dipole and NV mediated interactions. The Hamiltonian for the nuclear bath is

$$H_{\text{bath}} = -\hbar\mu_n \sum_j \mathbf{B}.\mathbf{I}_j + H_{\text{ndd}} + H_{\text{nnp}}. \tag{7}$$

Here, the first term is the sum of Zeeman interaction for all the spins, μ_n being the nuclear magnetic moment, and $\mathbf{I}_j$ is the j-th nuclear spin with $\mathbf{I} = (I_x, I_y, I_z)$. The second term is the dipole–dipole interaction, and the third term includes interactions mediated by the NV. The dipole–dipole interaction is given by

$$H_{\text{ndd}} = \sum_{j<k} \frac{\hbar^2 \mu_n^2}{r_{jk}^3} \left(\mathbf{I}^j \cdot \mathbf{I}^k - 3 \frac{(\mathbf{I}^j \cdot \mathbf{r}_{jk})(\mathbf{I}^k \cdot \mathbf{r}_{jk})}{r_{jk}^2} \right), \tag{8}$$

Here, $\mathbf{r}_{jk}$, is the distance vector between a pair of nuclear spins. The details of this interaction is discussed in Abragam (1983).

For proximal nuclear spins, the hyperfine interaction can also mediate spin flip-flop interactions, as discussed in Appendix B. The nuclear spin–spin interaction in this case is given by

$$H_{\text{nnp}} = \hbar \frac{(3m_s^2 - 2)}{4\Delta} \sum_{j \neq k} (\mathrm{A}^{\mathrm{j}}_{-}.\mathrm{I}^{\mathrm{j}})(\mathrm{A}^{\mathrm{k}}_{+}.\mathrm{I}^{\mathrm{k}}), \tag{9}$$

where $A_{\pm}^{j,k}$ are the off-diagonal terms of the hyperfine interaction tensor between the j,k-th nuclear spin and the NV. Due to the large zero-field splitting (Δ), this term is only dominant for ^{13}C nuclear spins in the first few coordinate shells, where the hyperfine interaction is large.

Even for modest fields (>1 Gauss), the nuclear Zeeman energy becomes significantly higher than nuclear spin–spin interaction strength. As a result, nuclear spins flip in pairs to conserve the Zeeman energy and we only focus on the energy conserving (or secular) part of the spin bath interactions. Under this approximation, both Eq. (8) and (9) can be approximated by

$$H_{\text{nn}} \approx \sum_{j<k} \hbar \Omega_{n,jk} (I_-^j I_+^k + \text{c.c.}) + \hbar \epsilon_{jk} I_z^j I_z^k, \tag{10}$$

where $\Omega_{n,jk}$ gives the strength of flip-flop interaction between a spin pair, and ϵ_{jk} corresponds to a local static field. Thus, in the secular approximation the nuclear spin interactions can be described by an XXZ model for spin–spin interactions.

2.5 Mechanism for Nuclear Spin Cooling

We now investigate how the electronic (i.e., fast) and hyperfine (i.e., intermediate) timescale interactions collaborate to further suppress the slow nuclear bath dynamics, leading to trapping the nuclear bath in configuration space. We also study how the nuclear bath interactions described in Section 2.4 influence the trapping quality.

The nuclear spins flip-flop around in pairs due to spin bath interactions, and the $I_+^j I_-^k$ terms can be mapped to a pseudospin 1/2 system, as illustrated in Fig. 5. For a dipole–dipole interacting pair, the coefficient of $I_+^j I_-^k$ terms is of the order of $\hbar^2 \mu_n^2 / r_{jk}^3$, and for NV mediated interaction it is of the order $\hbar A_{+-}^j A_{-+}^k / 2\Delta$. It is equivalent to the Rabi frequency for the pseudospin 1/2 system, which we shall refer to by Ω_{n0}. In the absence of hyperfine interaction, the energy difference between the two spins involved in flip-flop states is given by their interactions with the rest of the spin bath.

In the presence of an electronic spin, there is a significant energy difference between two nuclear states that differ only by one spin flip-flop interaction. This energy difference is due to the difference between the hyperfine

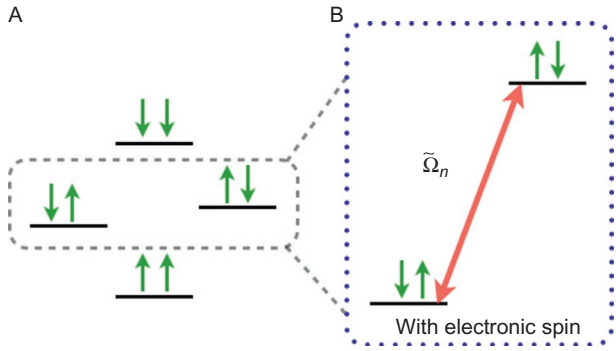

Figure 5 Model for nuclear spin–spin interaction induced spin flip-flop. Due to nuclear Zeeman interaction, this can be mapped to a pseudospin 1/2 system (a), with Rabi frequency Ω_n due to spin–spin interaction in the pair, and energy difference given by other spins in the bath. The presence of hyperfine interaction leads to a frequency shift of δ_f, suppressing such flip-flops in the dark state (b).

interaction of these two nuclear spin configurations with the electronic spin, and is shown in Fig. 5. The hyperfine interaction is typically orders of magnitude higher than nuclear dipole–dipole interaction. For example, assuming that both the hyperfine and nuclear spin–spin interactions are predominantly dipolar, all else being equal, it is enhanced by a factor of $\mu_e/\mu_n \sim 1000$, the ratio of gyromagnetic ratio of electron and nuclear spins. Thus the suppression due to hyperfine interaction can be very strong. If the next-closest nuclear spin configuration is $\delta = \delta_f$ from the resonant dark state ($\delta = 0$), this nuclear dipole–dipole interaction induced flip-flop is suppressed, and flip-flops occur at rate

$$\Omega_{n,D} = \Omega_{n0}^2/\widetilde{\Omega}_n, \tag{11}$$

where $\widetilde{\Omega}_n^2 = \Omega_{n0}^2 + \delta_f^2$ is the generalized Rabi frequency. This suppression should be significant in systems like NV centers, with a relatively sparse nuclear spin bath, hence significant δ_f for nearby spins. Appendix C shows the distribution of $\mathbf{\Omega}_{n0}$,$\mathbf{\Omega}_{nD}$ for realistic ^{13}C baths.

In spite of being suppressed, it is the only escape mechanism from the resonant nuclear spin configuration, so it cannot be ignored. It should be noted that in state $|0\rangle$, there is no suppression of bath interaction induced flip-flop due to the absence of hyperfine interaction, thus spins diffuse at rate $\mathbf{\Omega}_{n0}$. Weighing the two state dependent rates by their probabilities, the total spin diffusion rate due to interactions in the nuclear bath is given by

$$R_n = \mathbf{\Omega}_{n,D}(\rho_{DD} + \rho_{BB}) + \mathbf{\Omega}_{n,0}\rho_{00}. \tag{12}$$

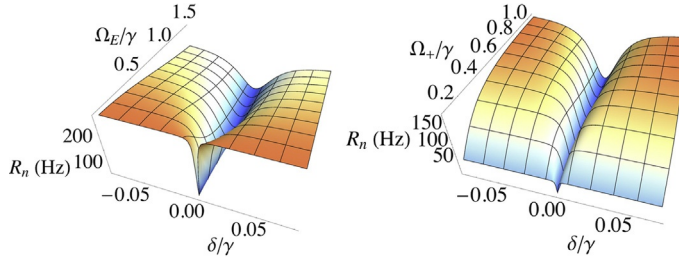

Figure 6 Nuclear diffusion rate (R_n, as defined in Eq. (12)) as a function of laser parameters. *Left*: R_n as a function of detuning (δ) and repump laser field strength (Ω_E) for $\Omega_+ = \sqrt{2} \times 0.8\gamma$. *Right*: R_n as a function of detuning (δ) and probe laser field strength (Ω_+), for $\Omega_E = 1\gamma$. For low laser powers ($\Omega_+ \ll \gamma$), very few nuclear spin configurations are subject to CPT cooling and nuclear diffusion is slow due to small population in the state $|0\rangle$. For higher Λ laser powers, nuclear diffusion is much faster.

Figure 6 shows the R_n nuclear diffusion rates as a function of the δ detuning and the $\boldsymbol{\Omega}_+$probe Rabi frequency. Here $\boldsymbol{\Omega}_n = 2\pi \times 230$ Hz, and $\delta_f = 2\pi \times 10$ kHz, and for simplicity we have assumed a constant distribution of δ in the CPT region, and the same δ_f for all δ all nuclear spin configuration states. This δ_f is equal to the average hyperfine interaction between a single nuclear spin and the NV. Details about the choice of these rates can be found in Appendix C. A quadratic dip in nuclear diffusion rate leads to the system being trapped in the nuclear spin configuration that leads to $\delta = 0$ for the electronic spin. We call this configuration $|D_{\text{nuc}}\rangle$ for pedagogical purposes, even though there are several configurations that lead to $\delta \sim 0$, particularly if we include nuclear spins weakly interacting with the NV. As we see in Fig. 6, diffusion out of $\delta = 0$ state is highly suppressed.

For low probe powers, there is very little nuclear diffusion due to low population in the state $|0\rangle$, and very slow escape from $|B\rangle$. Also, narrow CPT regions indicate that very few δ states, or nuclear spin configurations, are influenced by the presence of CPT lasers. Thus, if the nuclear spin is in the trapping region, it is strongly trapped, and outside there is no trapping of spin dynamics. Considering that there is no external force to push the nuclear spins towards the narrow selection of available configurations, the cooling process can be very slow for small laser powers.

For higher probe powers, a lot more spin configurations are influenced by the presence of CPT lasers. Large $\boldsymbol{\Omega}_+$ also indicates a larger contrast between the trapped and not-trapped nuclear spin configurations, and the spin diffusion is faster than in the case of low laser powers. We envision a typical experiment protocol to start with large laser powers in order to access a broader range of nuclear spin configurations, and reducing the laser powers

to further select nuclear spin configuration in order to perform efficient and fast laser cooling of the spin bath.

Since both nuclear diffusion and photon scattering rates depend on the same experimental parameters, it is instructive to find the relation between them. Rewriting the three ground state populations in terms of the excited state population ρ_{EE}, and using the relation for the photon scattering $R_p \approx \gamma_E \rho_{EE}$, with γ_E the scattering rate out of $|E\rangle$ (see Appendix A for details), we get the nuclear spin flip rate in the form

$$\begin{aligned} R_n &\approx \Omega_{n,D} + \left\{ \Omega_{n,0} \left(1 + \frac{\gamma + \gamma_{ce}}{R_E} \right) - \Omega_{n,D} \left(2 + \frac{\gamma + \gamma_{ce}}{R_E} \right) \right\} \rho_{EE} \\ &= \Omega_{n,D} + \left\{ \frac{\Omega_{n,0} - 2\Omega_{n,D}}{\gamma + \gamma_{ce}} + \frac{\Omega_{n,0} - \Omega_{n,D}}{R_E} \right\} R_p, \end{aligned} \tag{13}$$

i.e., as a function of the photon scattering rate R_p. Thus, the nuclear diffusion rate can be broken into two parts: one that is the intrinsic bath diffusion rate, and a second rate that is mediated by photon scattering. This is different from the exclusively photon scattering assisted diffusion mechanisms proposed in earlier work on nuclear spin diffusion (Issler et al., 2010; Wang et al., 2014). We believe that apart from the special case of nearby ^{13}C spins, the suppression of dipolar bath dynamics[3] is due to state dependent suppression as discussed above. The spin flip-flop process proposed by us also accounts for experimentally observed better cooling on the edges of the Overhauser distribution and a more discrete spin bath (such as the case for ^{14}N spin) due to large δ_f. In reality, the mechanism for laser cooling of the ^{13}C bath is a combination of both, with hyperfine assisted processes dominating for strongly coupled, nearby spins, and intrinsic spin flip-flop dynamics for the sub MHz, weakly coupled bath. The theory described here can be modified easily to take into account other processes if needed. We would like to note that the model for nuclear spin cooling presented above gives a qualitative understanding of the process. We expect a model including a more complete electronic level scheme to potentially give quantitatively better results.

3. SIMULATING SPIN BATH COOLING

We derive now expressions for the probability density function of time interval between successive nuclear spin flip-flop events. We

[3] as opposed to nuclear spins with $I > 1/2$ that have a nuclear quadrupolar moment, and hence are strongly influenced by local electric fields.

demonstrate the anomalous nuclear spin diffusion and emergence of Lévy statistics in nuclear flip-flop time intervals through Monte-Carlo (MC) simulations of a random walk in the space of an effective B_{eff} magnetic field to be introduced below. We discuss how the nuclear spin bath can get trapped in a certain spin configurations, leading to cooling of the spin bath. We conclude with ideas about measuring the cooled nuclear spin bath.

3.1 Random Walk Model for Nuclear Spin Diffusion

We now develop a random walk model for CPT in NV centers that focuses on inhomogeneous random walks in nuclear configuration space, deriving a simplified delay function that captures the necessary physics. The model discussed below is inspired by the classical random walk treatment of velocity selective coherent population trapping (VSCPT) in ultra cold atoms (Bardou et al., 2002). We would like to point out that this is not cooling in the sense of minimizing energy of the spin ensemble or cooling due to the presence of dissipative forces. Instead, the combined spin system gets trapped in a particular configuration state, thus narrowing the distribution of spin configurations.

The nuclear dynamics occur at much longer timescales than the electronic spin's interaction with the optical fields present, justifying a semiclassical treatment where we can replace the quantum description of hyperfine interaction by dynamics of a spin in a fictitious, classical magnetic field which models the Overhauser field. Here, we introduce B_{eff}, the difference of the applied and Overhauser fields. The quantum jumps leading to different nuclear spin configurations can be represented as steps in the B_{eff} space. Thus, the NV spin performs a random walk in B_{eff} space, with jumps between different δ states (corresponding to different nuclear spin configurations, hence B_{eff}) due to nuclear spin diffusion, each δ configuration leading to a jump rate given by Eq. (12).

Assuming an exponential distribution for the random time intervals for the nuclear bath to stay in the previously introduced $|D_{\text{nuc}}\rangle$ resonant dark state (corresponding to $\delta \approx 0$), the probability density function of the time interval (τ) to stay in a particular nuclear spin configuration is given by $W_{nD}(\tau,\delta) = R_n(\delta)e^{-R_n(\delta)\tau}$, where R_n is given by Eq. (12). Due to historical reasons related to photon arrival statistics, W_{nD} is also known as the delay function in literature (Bardou et al., 2002). Furthermore, assuming a constant density of nuclear spin configurations, the delay function becomes

$$W_{nD}(\tau_n) = \frac{1}{2\delta_{\text{trap}}} \int_{-\delta_{\text{trap}}}^{\delta_{\text{trap}}} W_{nD}(\tau, \delta) \mathrm{d}\delta. \tag{14}$$

We set $\delta_{\text{trap}} = R_{AB}/2$, where R_{AB} defined by Eq. (A.2) in Appendix A is the optical pumping rate on the $|B\rangle - |A_1\rangle$ transition, roughly equal to the width of the CPT dip. The analytic form of $W_{nD}(\tau)$ is complex, thus we leave it in the integral form for the sake of clarity. To this, we add the flip-flop rate outside the CPT region, where the nuclear bath dynamics is not suppressed. We call this the recycling region, and assume there is a constant nuclear spin diffusion rate in this B_{eff} region, which we call R_{nr}. This leads to a wait time distribution of $W_{n0} = R_{nr} e^{-R_{nr}\tau}$. Assigning them equal probabilities, the overall nuclear diffusion rate becomes

$$W_n(\tau) = \frac{1}{2}(W_{nD}(\tau) + W_{n0}(\tau)) \tag{15}$$

Long time intervals between successive nuclear spin flips would correspond to the nuclear spin being trapped in a particular configuration (in our case, $|D_{\text{nuc}}\rangle$). This is a result of the suppressed nuclear diffusion rates due to CPT of the electronic state. These events are included in the delay function due to our choice of δ interval. Outside δ_{trap}, the nuclear diffusion rate is not strongly δ dependent, as can be seen in the higher δ region of Fig. 6. This is due to the fact that the population in $|D,0\rangle$ saturates to a particular value, giving us a constant diffusion rate (R_{nr}). This region corresponds to fast nuclear diffusion with no CPT induced suppression, and hence no cooling. In Eq. (15), we assigned equal probability to the exponential distributions of trapping and recycling regions without loss of generality. The actual probabilistic weights of the two distributions depends on the details of the Overhauser field distribution of the NV under consideration. However, as we will see shortly, most quantitative details of the nuclear spin bath are actually contained in the exponent or power of the probability distributions.

3.2 MC Simulations for Nuclear Configurations

We now demonstrate the existence of Lévy statistics for the time intervals between Overhauser field changing ^{13}C spin flip-flops. In order to show this, we perform a MC simulation of dark time intervals using $W_n(\tau_n,\delta)$, showing a random walk of NV spin in δ space. Here, we have restricted δ to be in the region around the two-photon resonance ($-R_{AB} < \delta < R_{AB}$), since only the dynamics in this δ region gives rise to long dark times,

where the combined nuclear and electronic system is trapped in a state corresponding to a particular δ for $\tau_n \gg 1/\gamma$. For the purpose of this simulation, $\Omega_E = 1.0\gamma$, $\Omega_+ = \sqrt{2} \times 0.1\gamma$ and the nuclear bath parameters are $\Omega_{n0}/2\pi = 230$ Hz, and $\delta_f/2\pi = 10$ kHz. These laser parameters are chosen so that the electronic state is either $|D\rangle$ or $|0\rangle$ for simplicity. The nuclear bath parameters correspond to a typical scenario in natural abundance ^{13}C bath (1.1% concentration).

The nuclear spin diffusion rate of $\Omega_{n0}/2\pi = 230$ Hz corresponds to the next nearest neighbor dipolar interaction strength between two ^{13}C spins. A hyperfine interaction difference corresponding to $\delta_f/2\pi = 10$ kHz is chosen since it is close to the average hyperfine interaction with a single ^{13}C nuclear spin. Along with being the likely hyperfine difference, it also gives significant nuclear spin cooling. Having ^{13}C impurities on adjacent lattice sites along with a much larger hyperfine interaction difference is rare for natural abundance diamond samples, hence they are not chosen for this simulation. While possible, much larger δ_f are also not chosen since such flip-flops are highly suppressed in the $|D\rangle$ state (since $\Omega_{nD} \ll \Omega_{n0}$), and these nuclear spins are frozen in this configuration over realistic measurement times, and hence do not lead to escape from the $|D_{\text{nuc}}\rangle$ dark state configuration. On the other hand, small δ_f flip-flops are not suppressed irrespective of the electronic state of the NV, and thus our cooling scheme is ineffective in suppressing the diffusion of these (typically far away) nuclear spins. Thus, these parameters were chosen to correspond to the fastest diffusion rate out of $|D_{\text{nuc}}\rangle$ while also changing the Overhauser field significantly.

For a random δ, we pick a dark time interval from $W_n(\tau)$. At the end of the time interval, δ changes by $\pm\Delta\delta$ randomly. The time evolution of the nuclear spin bath is then simply a series of dark time intervals corresponding to a particular δ. A typical run showing about 200 steps in this random walk is shown in Fig. 7a. We notice long dark time intervals between δ-changing

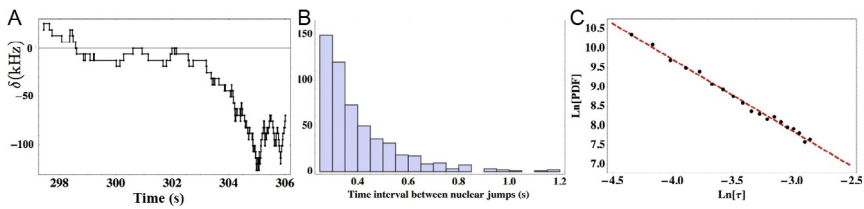

Figure 7 (a) Zoomed-in view of δ space random walk in time at $\delta_f/2\pi = 10$ kHz (b) Histogram of time intervals. (c) Power law fit.

jumps typically occurring for $\delta = 0$, as predicted by our theory. Furthermore, upon examining this random walk over different timescales we also notice a wide range of long dark time intervals, as seen in the histogram in Fig. 7b, indicating the "absence" of a steady state—a hallmark of Lévy statistics. This feature disappears at even longer timescales (of the order of $1/R_{n,D}$) indicating well-defined moments and a slow convergence to central limit theorem (Mantegna and Stanley, 1994). In the region $1/\Omega_{n,0} \ll \tau \ll 1/\Omega_{n,D}$, the histogram of time intervals has a power law form with τ^{α}, $\alpha = -1.7 \pm 0.1$, as shown in Fig. 7c. This indicates a power law probability density function(PDF) for dark time intervals.

There are several nuclear spin configurations corresponding to different δ in this CPT region. For the simulations, we assume a uniform distribution of equal δ states for simplicity, since the cooling is limited by the most likely and *fastest* diffusion rate out of the $|D_{nuc}\rangle$ configuration. For our choice of laser parameters, this uniform distribution corresponds to ~ 150 δ-configuration states in the trapping region. Furthermore, simulations with a realistic distribution of δ states for natural abundance ^{13}C samples give results consistent with uniform δ distributions for these parameters, albeit with a higher power for the power law PDF region, as we discuss now.

3.3 Prospects of Lévy Flights in ^{13}C Spin Bath Diffusion

The random walk theory of nuclear diffusion discussed above is very general and can be applied to any central spin system where there is an electronic CPT state, suppressing nuclear dynamics, for example in self-assembled quantum dots (Issler et al., 2010), or cooling the ^{14}N nuclear spin of an NV center (Togan et al., 2011), where nuclear quadrupolar interactions are dominant. In general, there are two major requirements for efficient nuclear spin bath cooling using CPT schemes:

1. Large hyperfine interaction compared to nuclear bath interactions, enabling diffusion suppression depending on the electronic state ($\Omega_{nD} \ll \Omega_{n0}$).
2. Small density of states of the nuclear spin configuration, ensuring that there is significant difference between the diffusion rates in the selected δ state versus all others. This enables the trapping of fewer nuclear spin configurations, making this cooling scheme more effective.

The conditions for power law behavior in nuclear spin diffusion are more stringent. Along with good conditions for laser cooling, it is essential to have a large number of possible nuclear spin configurations inside the CPT

region. This is because power laws in diffusion are a direct consequence of integral over several different exponential decays. A typical power law PDF will have the form $W_n(\tau) = A\tau^{-\alpha}$, where $\alpha > 1$, and A is the normalizing constant. Simple analysis reveals that mean and higher moments diverge for $\alpha < 2$, and variance and higher moments diverge for $\alpha < 3$. Such probability distributions with diverging variances lead to deviations from the Central Limit Theorem, which implies that the distribution of stochastic trajectories drawn from a distribution with a well-defined mean and variance would be Gaussian. This suggests that as we collect more data (in our case, observe nuclear configuration random walk over longer timescales), the variance would continue to grow. The understudying statistics is commonly known as Lévy flights (or Lévy statistics), and indicates probability of unlikely events is significant, and in fact dominates the dynamics of the system.

Figure 8 shows the statistical result of several MC simulations of the type discussed earlier, but for different δ_f, thus changing the number of states being summed over in the trapping region. In all cases shown here, we have a power law. At much larger δ_f, we simply have the sum over very few exponentials, and the long τ events become very rare, even though they dominate the dynamics. For much smaller δ_f, the power law behavior extends for less than a decade over τ, leading to large uncertainty in power law fitting.

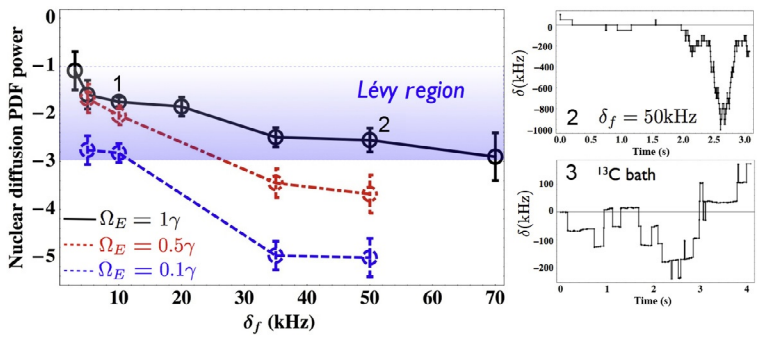

Figure 8 Power law study showing Lévy region. The *left panel* reports the power of the PDF obtained after MC simulations of nuclear dynamics for various δ_f and Ω_E. We notice that the power decreases as δ_f increases or Ω_E decreases. This is due to the availability of fewer nuclear spin configurations in the trapping region. While a typical MC run for data point 1 is shown in Fig. 7a, for data point 2 it is shown in the *upper right panel*. We notice that larger δ_f gives better trapping, even though we do not have Lévy flights. On the *lower right panel,* we also show the MC simulation of a realistic ^{13}C bath showing suppression of large δ_f states.

The requirement for power law PDF, however, is in contradiction with the condition for efficient laser cooling. We discuss two extreme cases to clarify this. On one extreme, in the case of ^{13}C spins very close to the NV center, there is a large difference between the hyperfine interactions of different configurations, and (NV induced) spin flip-flop interactions. As a result, such bath spins would be frozen in the desired configuration via our laser cooling scheme. However, due to the large hyperfine difference between very few spins, one has discrete, well-separated δ levels. The difference between successive δ states can be larger than the CPT width and summing over them does not give a power law—even though it gives us very efficient laser cooling. On the other extreme, we could consider the much larger spin bath formed by ^{13}C spins weakly coupled to the NV center. While these would give us an almost continuum of δ states inside the CPT region, due to the small hyperfine interaction difference between different configurations, there is minimal suppression of spin bath dynamics, making laser cooling ineffective. Furthermore, the probability distributions must be of power law form for well over a decade in time intervals to clearly measure the power. This requires a large difference between the suppressed and not suppressed spin diffusion rates. Thus, a spin bath with δ-level distribution well separated from the two extremes discussed above (with $10\ \text{kHz} < \delta_f/2\pi < 100\ \text{kHz}$) is ideal to observe Lévy statistics, and it is possible to find such environments in NVs with natural abundance ^{13}C samples. Both the hyperfine and the ^{13}C spin bath interactions are predominantly of dipole–dipole form, leading to a large suppression of bath dynamics due to difference in gyromagnetic ratio. Also, the natural concentration of ^{13}C spins is small giving us a sparse nuclear spin bath with the possibility of some well separated, but still a large number of δ states. These features make the ^{13}C nuclear spin bath a good candidate for observing efficient CPT (or laser) cooling of the nuclear spin bath.

3.4 Measuring the Laser Cooled Spin Bath

As shown earlier, MC simulations of nuclear spin dynamics in configuration space demonstrate the nuclear spin bath getting trapped in particular spin configurations for long times. We now comment on ways to demonstrate cooling of the spin bath. Here, we borrow techniques from laser cooling of atoms, where time-of-flight measurements were used to demonstrate narrowing of the velocity distribution of a gas of ultra-cold atoms. In the case of cold atoms, a gas of trapped atoms is released and then imaged using

absorption spectroscopy after some time. The position distribution of the atomic ensemble gives us the velocity distribution of the trapped gas. Since we have an ensemble of atoms, a single (albeit destructive) measurement is sufficient to establish the momentum distribution of atoms.

In principle, we can perform fast electron spin resonance spectroscopy (e.g., in Dréau et al., 2014) or dark state spectroscopy (as done in Togan et al., 2011) after laser cooling of the bath. Here, spectroscopy involves either sweeping the magnetic field, or laser (or microwave) frequency, and measuring photoluminescence. As we change δ, the NV gets pumped into an optically dark state, or another electronic state only for certain B_{eff}, giving us a signal proportional to the instantaneous Overhauser field. Unlike atomic ensembles, we are dealing with a *single* quantum emitter. Hence, we need to perform repeated measurements in order to measure the Overhauser field distribution. Measuring the Overhauser field spectrum before and after laser cooling of the bath would demonstrate the narrowing, and hence cooling of the spin bath, as was demonstrated in Togan et al. (2011).

In order to demonstrate cooling of the spin bath, the authors of that reference used the nuclear spin configuration dependent photon scattering rate. In principle, one could use the same photons to measure the slow dynamics of the nuclear bath itself. Measuring the rate of nuclear bath dynamics (R_{n0},R_{nD}) gives us quantitative information about the interactions in the complex spin bath that is evolving far from equilibrium. We now focus on how to extract nuclear spin bath diffusion rates by measuring photon arrival time intervals.

4. PHOTON STATISTICS

In Section 3, we derived how the nuclear spin bath can get trapped in a certain spin configuration, leading to cooling of the spin bath. We now elaborate on how to experimentally extract the properties of the ^{13}C nuclear bath by using fluorescence from the NV center. Successive photon scattering events from the NV center after time intervals much greater than the inverse of the spontaneous emission rates indicate an escape from the electronic dark state. Hence, time intervals between photon detection events forms a natural measurement device for observing the slow nuclear bath dynamics associated with the electronic dark state.

However, photon scattering is itself a random process, and the rates of photon scattering are typically orders of magnitude higher than nuclear diffusion rates, masking any effects due to bath dynamics outside the resonant

dark state. In the following, we model the photon scattering as a random walk in δ space, and discuss coupled photon nuclear spin dynamics and the possibility of analyzing the suppressed nuclear diffusion by measuring photons.

In particular, we show that while the photon statistics do give critical insight into the nuclear spin dynamics, the presence of Lévy statistics in the photons do not directly indicate nuclear spin cooling.

4.1 Photon Random Walk

We focus on the region around the two-photon resonance, $\delta \propto B_{\text{eff}} = 0$, where the rate to escape the electronic dark state (and hence observe photon fluorescence) depends on δ^2 (Aspect et al., 1989). Around $\delta = 0$, this rate is given by $R_{\text{BD}} = \delta^2 / R_{AB}$. Ideally this rate approaches zero at resonance, allowing the spin to remain in the dark state for very long times. However, as discussed in the previous section, along with a δ −dependent R_{BD}, there is slow dynamics due to nuclear spin diffusion. We ignore it for the time being, assuming it is slower than the time intervals (τ) in consideration. The overall photon jump rate out of the electronic dark state is therefore given by

$$R_D(\delta) = R_{BD} = \frac{(\gamma + \gamma_0 + \Gamma)}{\Omega_+^2}\delta^2 \tag{16}$$

Once out of the electronic dark state, the NV fluoresces as it undergoes the $|A_1\rangle \rightarrow |B\rangle$ transition (at rate $\gamma_A \rho_{AA}$), or the $|E_\gamma\rangle \rightarrow |0\rangle$ transition (at rate $\gamma_E \rho_{EE}$), as discussed in Appendix A. Being only 2.87 GHz apart, the detector cannot distinguish between photons from these two transitions, the total photon scattering rate is simply the sum of these. For simplicity, we divide the B_{eff} range set by the Overhauser field distribution into two regions: the trapping region, where photon detection rate is limited by the δ-dependent escape rate out of the dark state, and a recycling region, where photon detection rate is constant, equal to $R_{\text{nres}} = \eta(\gamma_E \rho_{EE} + \gamma_A \rho_{AA})$, with η being the photon collection efficiency of the detector, and ρ_{EE},ρ_{AA} being evaluated at $\delta \gg \delta_{\text{trap}}$. This constant off-resonance photon detection rate can be easily be measured in an actual experiment.

Assuming an exponential distribution for the random time intervals for the NV electronic spin to stay in the dark state, the probability density $W_{pD}(\tau, \delta) = R_D(\delta) e^{-R_D(\delta)\tau}$. Furthermore, assuming a constant density of δ as before, the time interval probability density function becomes

$$\begin{aligned} W_{pD}(\tau) &= \frac{1}{2\delta_{\text{trap}}}\int_{-\delta_{\text{trap}}}^{\delta_{\text{trap}}} W_{pD}(\tau,\delta)\rho_{DD}(\delta)\mathrm{d}\delta, \\ &= \frac{1}{2\delta_{\text{trap}}}\mathrm{e}^{-R_s\tau}\int_{-\delta_{\text{trap}}}^{\delta_{\text{trap}}}\left(\frac{\delta^2}{R_{AB}}\right)\mathrm{e}^{-\delta^2\tau/R_{AB}}\rho_{DD}(\delta)\mathrm{d}\delta. \end{aligned} \tag{17}$$

Here, $\rho_{DD}(\delta)$ is the population in dark state at detuning δ, and δ_{trap} is approximately the maximum δ for which the system can remain trapped in the dark state. We set $\delta_{\text{trap}} = R_{AB}/2$, as before. The analytic form of $W_{pD}(\tau)$ is an incomplete Gamma function, but we leave it in the integral form for the sake of clarity.

We add to this the photon scattering rate in the recycling region. Once out of the dark state, photon scattering occurs at much faster timescales, and does not change the overall distribution much over long time intervals. This process corresponds to a wait-time distribution of $W_{p0}(\tau) = R_{\text{nres}}\mathrm{e}^{-R_{\text{nres}}\tau}$. Following the same reasoning as done for spin configurations, the overall probability density of detecting photons is therefore

$$W_p(\tau) = \frac{1}{2}\big(W_{pD}(\tau) + W_{p0}(\tau)\big). \tag{18}$$

Figure 9 shows MC simulations of nuclear and photon statistics for different nuclear diffusion rates. In the top panel, the nuclear diffusion rate is δ independent. Thus, there is a constant rate to go from one δ state to another in the trapping region. This corresponds to no trapping of nuclear spin configurations, and an exponential distribution of time interval to stay in a certain δ state (we call it τ_s). As opposed to this, the bottom panel shows the coupled dynamics for δ-dependent nuclear diffusion rate, consistent with our theory for nuclear spin cooling. As can be seen in the simulated random walk (red lines (gray in the print version)), in this case the nuclear spin gets trapped in configurations around $\delta = 0$ for long time intervals giving rise to a power law distribution in the probability to stay in the same δ state. In both cases, we have assumed the same δ dependent photon arrival time (τ_p) distribution, given by Eq. (18), but with $\tau \to \tau_p$. In general, $\tau_p \ll \tau_s$ unless the system is the neighborhood of the optically dark state, i.e., $\delta = 0$, which leads to Lévy flights behavior in photon arrival times, with long time intervals between photon arrivals.

From Fig. 9, it is clear that Lévy statistics in photon dark counts does not confirm nuclear spin bath cooling. It is not necessary for the nuclear spin diffusion rate to have a δ dependence in order to observe a power law

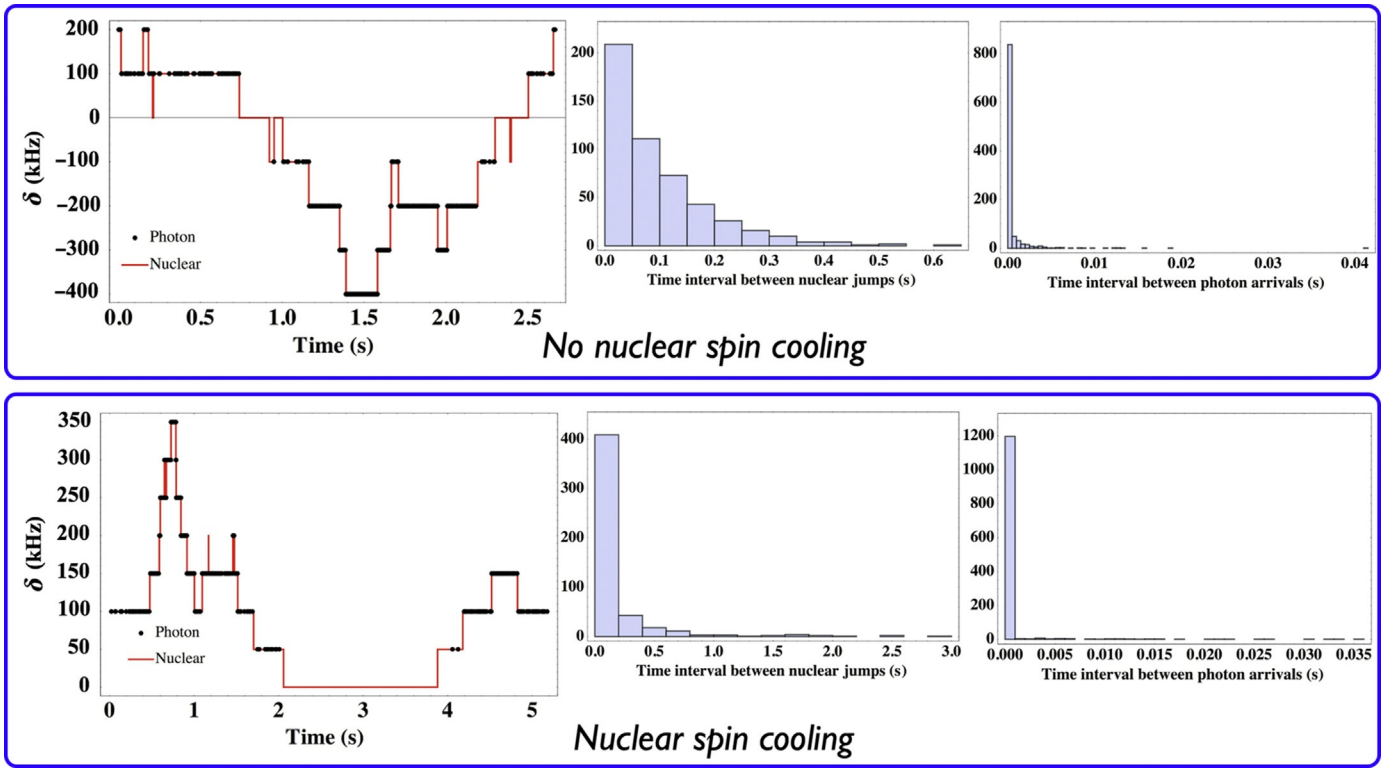

Figure 9 Photon arrival and nuclear spin jump events for different δ states around the optical dark state. The top panels indicate constant (δ independent) nuclear spin diffusion and the bottom panels indicate nuclear spins being trapped around δ=0 for long time intervals. The *left panels* report the temporal evolution of the δ detuning of the atomic state, as monitored on the photon arrivals (black dots) and the nuclear diffusion (red (gray in the print version) lines). The *center* and *right panels* report the distributions of the time intervals between nuclear jumps and photon arrivals. In both upper and lower cases, the photon arrival statistics show long time intervals consistent with Lévy flights.

distribution in photon dark time intervals. However, one needs a δ dependent nuclear diffusion rate in order to CPT cool the spin bath. A nonzero nuclear diffusion rate is sufficient to enable a photon random walk in δ space. This highlights the crucial difference from VSCPT cooling in cold atoms. In VSCPT, *each* photon emission event is accompanied by a recoil kick to the atom being cooled. Since momentum diffusion is completely dependent on the photon emission, there is only one random process. In the nuclear spin CPT scheme, Doppler shift detuning is replaced by Overhauser field detuning. Thus, instead of velocity selection, we have Overhauser field selection. However, as is clear from Eq. (13), while the nuclear diffusion rate depends on similar parameters as photon scattering, it is not proportional to the photon scattering rate. As also supported by our microscopic theory, a photon emission event does not directly lead to a change in nuclear spin configuration. In fact, they are two *independent* stochastic processes that depend on the same parameters. This insight is also supported by MC simulations of these two random processes as shown in Fig. 9. We now develop the analytical framework to deal with these coupled random processes.

4.2 Coupled Nuclear Spin-Photon Random Walks

As established by now, there are two random processes that lead to a particular time interval between two fluorescence events—the δ dependent photon scattering rate, and the δ changing nuclear bath interactions. However, we can only observe photons. In order to understand how nuclear diffusion (as discussed in Section 3.1) changes photon arrival statistics, we now develop a simple Markov chain model for the photon scattering rate, provided there is nuclear spin diffusion in the system.

For consistency, we use subscript D to denote the trapping region ($|\delta| < \delta_{\text{trap}} = R_{AB}$), where both nuclear diffusion ($R_{nD} = R_n(\delta)$) and photon scattering rates ($R_{pD} \approx R_{BD}(\delta)$) are δ dependent, and subscript 0 for the recycling region outside the CPT region, where both these rates are constant ($R_{n0} = R_n(\delta_r), R_{p0} = \eta R_p(\delta_r)$. We also define $P_{\text{d(nd)},0}$, the probability to detect (not detect) a photon in the recycling region, and $P_{\text{d(nd)},D}$ for the trapping region. Figure 10 describes the Markov chain model to describe this coupled process. Nuclear spin flip event occur at rate R_{n0}, R_{nD}, depending on the state, as shown by green (gray in the print version) arrows in Fig. 10. Thus, $R_{nD} < R_{n0}$ leads to trapping in the desired configuration. Similarly, depending on the nuclear configuration being 0 or D, the photon detection rates are R_{p0}, R_{pD} respectively, as shown by blue (black in the print version) arrows in Fig. 10. The four joint probabilities evolve as

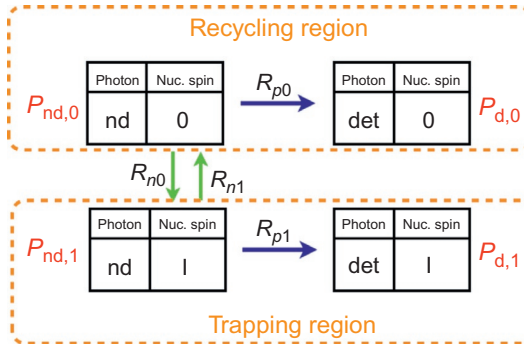

Figure 10 Markov chain model for nuclear spin dependent photon scattering events.

$$\begin{aligned}
\dot{P}_{\mathrm{nd},0} &= -(R_{n0}+R_{p0})P_{\mathrm{nd},0}(\tau)+R_{nD}P_{\mathrm{nd},D}(\tau),\\
\dot{P}_{\mathrm{nd},D} &= R_{n0}P_{\mathrm{nd},0}(\tau)-(R_{pD}+R_{nD})P_{\mathrm{nd},D}(\tau),\\
\dot{P}_{\mathrm{d},0} &= R_{p0}P_{\mathrm{nd},0}(\tau),\\
\dot{P}_{\mathrm{d},D} &= R_{pD}P_{\mathrm{nd},D}(\tau).
\end{aligned}$$

Here, we have assumed that once the photon is detected, the system reinitializes itself into the nd-state in order to be consistent with Markov approximation for photon detection events. Assuming the system starts in state nd,0, we can solve the above system of equations to get the probabilities

$$\begin{aligned}
P_{\mathrm{nd},0}(\tau) &= \frac{\mathrm{e}^{-R_+\tau/2}}{2R_e}\left\{\mathrm{e}^{-R_e\tau/2}(R_e+R_-))+\mathrm{e}^{R_e\tau/2}(R_e-R_-))\right\},\\
P_{\mathrm{nd},D}(\tau) &= \frac{\mathrm{e}^{-R_+\tau/2}}{R_e}\left\{R_{n0}\left(\mathrm{e}^{R_e\tau/2}-\mathrm{e}^{-R_e\tau/2}\right)\right\}.
\end{aligned} \tag{19}$$

where $R_\pm = R_{p0}+R_{n0}\pm(R_{pD}+R_{nD})$, and $R_e = \left(R_+^2-4(R_{pD}(R_{p0}+R_{n0})+R_{nD}R_{p0})\right)^{1/2}$. Since the photodetector is oblivious to nuclear configuration, the joint probability to detect photons evolves as $\dot{P}_{\mathrm{d}} = \dot{P}_{\mathrm{d},0}+\dot{P}_{\mathrm{d},D} = R_{p0}P_{\mathrm{nd},0}(\tau)+R_{pD}P_{\mathrm{nd},D}(\tau)$. $\dot{P}_{\mathrm{d}}$ is simply the joint PDF for the photon detection at time τ,

$$\begin{aligned}
W_{T,0}(\tau,\delta) &= \frac{\mathrm{e}^{-\frac{R_+\tau}{2}}}{2R_e}\left\{\mathrm{e}^{-\frac{R_e\tau}{2}}\left(R_{p0}(R_e+R_-)-2R_{pD}R_{n0}\right)\right.\\
&+ \left.\mathrm{e}^{\frac{R_e\tau}{2}}\left(R_{p0}(R_e-R_-)+2R_{pD}R_{n0}\right)\right\}.
\end{aligned} \tag{20}$$

Equation (20) is the more general form of $W_p(\tau)$, taking into account the varying nuclear diffusion rates. In Eq. (20), we assumed that once a photon

is detected, the system reinitializes itself into the (photon not-detected, nuclear spin not trapped) state. This is a reasonable assumption, given the fact that only a few of the available nuclear spin configurations are in the CPT region, where photon scattering rate approaches zero.

However, it is no longer the case for a laser-cooled nuclear spin ensemble. Here, with a large probability, all photon emission events occur while the nuclear spins remain in the trapping region. This can be incorporated into the previous model as a different initial condition: the system now reinitializes itself into the (photon not-detected, nuclear spin trapped) state. The solution to photon PDF now looks like

$$W_{T,D}(\tau,\delta) = \frac{e^{-\frac{R_+\tau}{2}}}{2R_e}\left\{e^{-\frac{R_e\tau}{2}}\left(R_{pD}(R_e-R_-)-2R_{p0}R_{nD}\right)\right. \\ \left. + \; e^{\frac{R_e\tau}{2}}\left(R_{pD}(R_e+R_-)+2R_{p0}R_{nD}\right)\right\}. \tag{21}$$

If we assume the initial state to be equal probability of being in the trapped or recycling regions (in order to be consistent with Eq. (18) and Eq. (15)), we get

$$W_T(\tau,\delta) = \frac{1}{2}\left(W_{T,D}(\tau,\delta) + W_{T,0}(\tau,\delta)\right) \tag{22}$$

Comparing Eqs. (20) and (21), we notice that while the exponentials remain the same, the coefficients of the exponentials change as we change the initial conditions. A linear combination of these two PDFs describes the statistics if the nuclear spin bath is between these two extremes, i.e., population is divided between the trapping and recycling region, as shown in Eq. (22). Figure 11 shows the resulting PDF for these three initial conditions. By looking at the PDFs over several decades, we can draw two main conclusions. Firstly, the probability to have long dark time intervals is significantly higher if the nuclear spin bath is in a trapped state. Secondly, while the deviation from power law at long-τ is identical for all three PDFs, the power law behavior starts at much shorter time intervals if the nuclear spin ensemble is in a trapped state.

4.3 Photon Statistics Dominated by Nuclear Dynamics

The derivations in Section 4.2 clarify that there is no clear demarkation between the photon and nuclear rates. This makes it hard to explicitly measure the nuclear diffusion rates while ignoring the affect of photon scattering

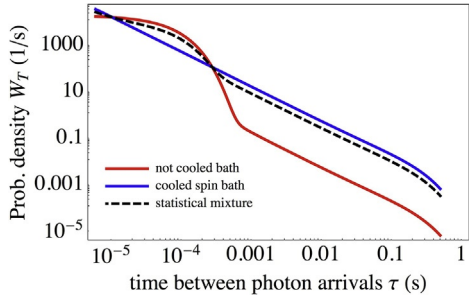

Figure 11 Photon arrival PDF for different initial conditions of the nuclear spin bath (blue (dark gray in the print version): trapping region (Eq. (21)), red (gray in the print version): recycling region (Eq. (20)), and dashed: equal mixture of the two (Eq. (22)) over several decades in dark time interval. While all PDFs are exponential for long and short time intervals, and power law ($\propto \tau^{-3/2}$) in the middle, the power law region for photon statistics stays over a longer τ region and is more likely to be observed if the nuclear spins are in the trapping region.

rates. This problem is further exacerbated by the fact that we integrate over all δ states. However, we can identify regions in laser parameter space where W_T is dominated by spin dynamics. As mentioned in Section 4.1, we can measure the photon wait-time distribution experimentally. Thus, we need to find situations where the photon statistics is dominated by nuclear spin dynamics. Figure 12 shows two such situations, where we plot the W_T photon arrival probability density as derived in Eq. (22), but for different repump laser powers corresponding to $\Omega_E = 1\gamma$ (upper panel), and 0.05γ (lower panel). For comparison, we also show the behavior of the W_p simple photon statistics as described by Eq. (18) (in red (dark gray in the print version)), and the W_n nuclear diffusion, as described by Eq. (15) (in green (dot-dashed line in the print version)). In both regimes of laser power, the long-τ photon statistics gives us quantitative information about nuclear dynamics.

For large pumping power (upper panel in Fig. 12), the photon scattering rate is typically very high, and the long time interval behavior of photon scattering rates is limited by nuclear spins diffusing out of the trapped region, as shown in Fig. 12a. This implies that the nuclear spin bath configuration changes before a photon can be emitted from the electronic dark state ($\delta \sim 0$). Thus the time interval between successive photon arrivals is approximately $1/R_{n1}(\delta \sim 0) + 1/R_{p1}(\delta_{\text{next}}) \approx 1/R_{n1}(\delta \sim 0)$, where δ_{next} is the δ state the nuclear spin diffused to out of the dark state. This is why both nuclear spin PDF (W_n, in green (dot-dashed line in the print version)), and total PDF (W_T, in black) are the same exponential, as seen in

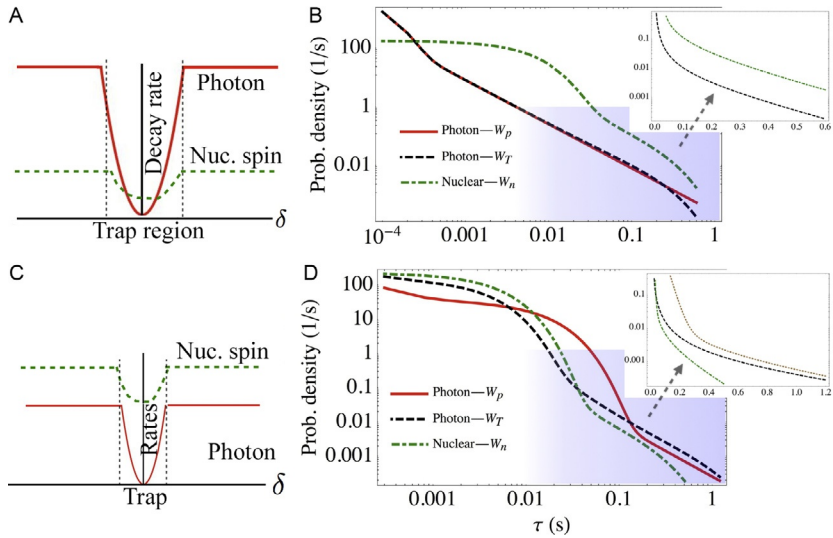

Figure 12 Interplay of photon scattering and nuclear diffusion for high ($\Omega_E = 1\gamma$ in upper panel) and low ($\Omega_E = 0.05\gamma$ in lower panel) repump laser power. The relative rates for photon scattering and nuclear diffusion are sketched on the left. On the right, we show the PDF of several processes over several decades in the dark time interval. The shaded areas are shown on a log-linear plot to elucidate exponential decays. The insets emphasize the long-time limit in a linear time plot. The upper brown (gray in the print version) curve in the bottom inset shows how the steady-state photon scattering rate would look like.

Fig. 12b. Thus, the exponential tail of the high pumping power photon PDF gives us the nuclear spin flip-flop rate out of the electronic dark state.

For low pumping power, the situation is very different. Here, the spin diffusion rates are higher than the photon scattering rates as shown in Fig. 12c. Thus, the spin distribution comes to an equilibrium in response to the laser and magnetic fields before photons are emitted. In the long time limit, the photon scattering rate would then be proportional to the probability to be in recycling region × photon scattering rate, $R_{p,ss} = R_{p0} \times \rho_{n0,ss}$, where $\rho_{n0,ss} = R_{n1}/(R_{n1} + R_{n0})$ is the steady state population in the recycling region. Figure 12d shows this exponential PDF ($W_{p,ss} = R_{p,ss} e^{-R_{p,ss}\tau}$, reported as the brown curve within the inset). Thus, while we cannot read off the nuclear rate directly in this case, in combination with the strong pumping limit (as discussed above) we can now learn the value of both, R_{n0} from the strong pumping limit and R_{n1} from the combination of R_{n0} and R_{n1} in the low pumping limit. Note, however, that Fig. 12 also shows that the nuclear spin cooling is not very efficient for low laser powers.

We realize that just by varying the laser power, we can indeed use photons to not just to cool the bath, but also to measure properties of the nuclear spin bath that are hard to measure otherwise. Along with proper characterization of the laser–NV interaction, and technical details (collection efficiency, etc.,), we can vary laser powers and measure the wait-time distribution to extract information about the bath (Ω_{n0},Ω_{nd}). A large difference between these two rates indicate NVs whose nuclear bath can be cooled efficiently using the CPT cooling technique discussed earlier.

5. CONCLUSION

We have discussed for a diamond NV center the physical system and methods to treat this as a type of central spin system; we have clarified the relationship between measurement of electron dominated photon statistics and the dynamics and manipulation of the nuclear spin bath. Despite the fact that there is no direct proportionality between emitted photons and nuclear spin flips, it is possible to draw clear conclusions about the nuclear bath and its momentary temperature. This knowledge can then be used for cooling this bath—or freezing it to a single state, depending on the parameters. In addition, it is possible to choose the parameters such as to allow for a measurement of Lévy statistics of both the emitted photons and the nuclear spin flips in the bath of this particular single quantum system. In addition, we showed here how a Markov chain model can be used to gain theoretical information about this complex system, which can be generalized to similar systems in a straightforward manner.

One of the most important open questions left by this work relates to the anisotropy of the dipolar interaction in this system: There are, for each nuclear spin, two competing quantization axes, the direction of the field caused by the electron spin, which can be different for each nuclear spin, and the external quantization axis of the full system, i.e., the external B-field. While this is indirectly taken into account in the averaging connected to our probabilistic treatment, it would be interesting to understand the detailed influence of this geometry.

In addition, the research discussed here will be used to construct a feedback scheme to further cool down the spin bath. The information gained from the measurement can, in this case, inform system manipulation by changing the laser intensity, the strength and/or the direction of the outside magnetic field. The latter, change of magnetic field direction, might be

particularly interesting when taking into account the above-mentioned anisotropy in more detail, for example, by potentially rectifying the different quantization axes for differently located nuclear spins.

ACKNOWLEDGMENTS

We acknowledge stimulating discussions with E. Bauch, J. Lee, E. Kessler, M. Goldman, A. Pick, and A. Aspect. This work is supported by US National Science Foundation and the US Army Research Office.

APPENDIX A. NV–LASER INTERACTION DETAILS

In the following, we solve for the steady state of the NV spin interacting with the laser fields addressing the open Λ system. After making the rotating wave approximations, the Hamiltonian for laser–NV interaction (in basis $|A\rangle,|B\rangle,|D\rangle,|E_y\rangle,|0\rangle$) is

$$H_{\text{opt}} = \hbar \begin{bmatrix} 0 & -\Omega_+/2 & 0 & 0 & 0 \\ -\Omega_+/2 & 0 & -\delta/2 & 0 & 0 \\ 0 & -\delta/2 & 0 & 0 & 0 \\ 0 & 0 & 0 & 0 & -\Omega_E/2 \\ 0 & 0 & 0 & -\Omega_E/2 & 0 \end{bmatrix}. \tag{A.1}$$

The Louvillian takes into account spontaneous emission (at rate γ from $|A\rangle$ to the Λ ground states, and from $|E\rangle$ to $|0\rangle$, at cross rates γ_0 from $|A\rangle$ to $|0\rangle$, and γ_{ce} *from* $|E\rangle$ to Λ ground), and dephasing at rate Γ from the two excited states, and is given by

$$\mathcal{L}[\rho] = \begin{bmatrix} -\gamma_A\rho_{AA} & -\frac{\Gamma_A}{2}\rho_{AB} & -\frac{\Gamma_A}{2}\rho_{AD} & -\frac{(\Gamma_A+\Gamma_E)}{2}\rho_{AE} & -\frac{\Gamma_A}{2}\rho_{A0} \\ -\frac{\Gamma_A}{2}\rho_{BA} & \frac{\gamma}{2}\rho_{AA}+\frac{\gamma_{ce}}{2}\rho_{EE} & 0 & -\frac{\Gamma_E}{2}\rho_{BE} & 0 \\ -\frac{\Gamma_A}{2}\rho_{DA} & 0 & \frac{\gamma}{2}\rho_{AA}+\frac{\gamma_{ce}}{2}\rho_{EE} & -\frac{\Gamma_E}{2}\rho_{DE} & 0 \\ -\frac{(\Gamma_A+\Gamma_E)}{2}\rho_{EA} & -\frac{\Gamma_E}{2}\rho_{EB} & -\frac{\Gamma_E}{2}\rho_{ED} & -\gamma_E\rho_{EE} & -\frac{\Gamma_E}{2}\rho_{E0} \\ -\frac{\Gamma_A}{2}\rho_{0A} & 0 & 0 & -\frac{\Gamma_E}{2}\rho_{0E} & \gamma_0\rho_{AA}+\gamma\rho_{EE} \end{bmatrix}.$$

Here, we have introduced variables $\gamma_A = \gamma + \gamma_0$, $\gamma_E = \gamma_{ce} + \gamma$, $\Gamma_A = \gamma_A + \Gamma$ and $\Gamma_E = \gamma_E + \Gamma$ for brevity.

We obtain the equations of motion for the density matrix using the standard Master equation formalism:$\dot{\rho} = -(i/\hbar)[H,\rho] + \mathcal{L}[\rho]$. Such master equations are typically solved using numerical methods, for example wave-function MC simulations (Mølmer et al., 1993). However, we are interested in the long-time behavior of the system ($t \gg 1/\gamma$), uncovering nuclear diffusion and Lévy statistics, making the problem computationally intensive. In order to study the statistics of the sequence of quantum jumps giving us intermittent fluorescence photons, it is convenient to use the "delay function" formalism (see, e.g., Cohen-Tannoudji and Dalibard, 1986; Zoller et al., 1987), which we derive for our case in the following. We assume that over the timescales of nuclear diffusion, the system (NV spin interacting with lasers) has evolved into a steady state. Since the electronic spin adjusts relatively quickly to the changes in the nuclear environment, we can justify a steady state treatment. Assuming steady state values for coherences, the system of equations governing the populations becomes

$$\begin{bmatrix} \dot{\rho}_{AA} \\ \dot{\rho}_{BB} \\ \dot{\rho}_{DD} \\ \dot{\rho}_{EE} \\ \dot{\rho}_{00} \end{bmatrix} = \begin{bmatrix} -(\gamma_A + R_{AB}) & R_{AB} - \frac{\delta^2}{\Omega_+^2} R_{AB} & \frac{\delta^2}{\Omega_+^2} R_{AB} & 0 & 0 \\ (\gamma_A + R_{AB}) & -R_{AB} + \frac{\delta^2}{\Omega_+^2} R_{AB} - R_{BD} & -\frac{\delta^2}{\Omega_+^2} R_{AB} + R_{BD} & \gamma_{ce} & 0 \\ \gamma & R_{BD} & -R_{BD} & \gamma_{ce} & 0 \\ 0 & 0 & 0 & -\gamma_E - R_E & R_E \\ \gamma_0 & 0 & 0 & \gamma + R_E & -R_E \end{bmatrix} \begin{bmatrix} \rho_{AA} \\ \rho_{BB} \\ \rho_{DD} \\ \rho_{EE} \\ \rho_{00} \end{bmatrix},$$

where the optical pumping rates are

$$R_{AB} = \Omega_+{}^2/\Gamma_A; \quad R_E = \Omega_E^2/\Gamma_E; \quad R_{BD} = \delta^2/R_{AB}. \tag{A.2}$$

Here, we have ignored the terms proportional to δ/Γ_A, since it is $\ll 1$ over the detuning range of interest ($-R_{AB} \leq \delta \leq R_{AB}$). Under the approximation $\gamma_{ce}/\gamma_0 \ll 1$, we can simplify the steady state populations to

$$\rho_{EE} = A_E \frac{\delta^2}{\delta^2 + \delta_0^2}, \tag{A.3}$$

$$\rho_{00} = \left(1 + \frac{\gamma + \gamma_{ce}}{R_E}\right)\rho_{EE}, \tag{A.4}$$

$$\rho_{BB} + \rho_{DD} = 1 - \left(2 + \frac{\gamma + \gamma_{ce}}{R_E}\right)\rho_{EE}, \tag{A.5}$$

where

$$A_E \approx \frac{1}{2+2\dfrac{\gamma_{ce}(\gamma+\gamma_0)}{\gamma_0 R_{AB}}+\dfrac{\gamma+\gamma_{ce}}{R_E}}, \tag{A.6}$$

$$\delta_0^2 \approx \frac{\gamma_{ce}}{4\gamma_0\dfrac{\gamma_{ce}}{\gamma_0}+\dfrac{\gamma}{4(\gamma+\gamma_0)}\left(\dfrac{2R_{AB}}{\gamma}+\dfrac{R_{AB}}{R_E}\right)}\cdot\frac{R_{AB}^2}{}. \tag{A.7}$$

Figure 3a and b shows the steady state population in several ground electronic states as a function of detuning δ and Rabi frequency Ω_E.

Once out of the dark state, the NV fluoresces as it undergoes the $|A\rangle \rightarrow |B\rangle$ transition with photon scattering rate $\gamma_A\rho_{AA}$), or the $|E_y\rangle \rightarrow\rangle|0\rangle$ transition, with the corresponding photon scattering rate being $\gamma_E\rho_{EE}$). Being only 2.87 GHz apart, the detector cannot distinguish between photons from these two transitions and the total photon scattering rate is simply the sum of these. Since not all the photons emitted are detected, the photon detection rate is a fraction (η) of photon scattering rate, and is determined by the efficiency of the detection setup ($\eta \ll 1$). The photon detection rate is therefore

$$R_{ps} = \eta(\gamma_E\rho_{EE} + \gamma_A\rho_{AA}) \approx \eta\gamma_E\rho_{EE}. \tag{A.8}$$

We would like to note that a simple rate equation model was developed to study the steady state because the coherences between different electronic states do not affect the overall population distribution over the long timescales in consideration here. We confirmed this by comparing this solution to the solution of the entire density matrix for the case of a single spin 1/2 nuclear spin. Moreover, we also confirmed that there are no significant effects due to coherences between different nuclear manifolds.

APPENDIX B. DETAILS OF HYPERFINE INTERACTION

In this section, we derive the correction to our simple model for hyperfine interaction discussed in Section 2.3 that leads to energy splittings and interactions in the nuclear bath Hamiltonian. We comment on the conditions when these terms can be ignored. As discussed in Eq. (3), the total Hamiltonian for our central spin system is given by

$$H = H_{\text{bath}} + \hbar\Delta S_z^2 + \hbar\mu_e \vec{S}\,.\,\vec{B} + \hbar\sum_{j,\mu,\nu} S_\mu A^j_{\mu\nu} I^j_\nu. \tag{B.1}$$

Here, we have left the hyperfine tensor in a general form in order to take into account both contact and dipole–dipole interaction. In this section, we shall ignore the pure bath dynamics, and treat the off-axis hyperfine and Zeeman interaction as a perturbation. Thus, we break the Hamiltonian into H_0, and a small perturbation V with

$$H_0 = \hbar\Delta S_z^2 + \hbar\mu_e S_z B_z + \hbar\sum_{j,\nu} S_z A_{z\nu} I_\nu^j, \tag{B.2}$$

$$V = \frac{1}{2}\hbar\mu_e(B_+ S_- + B_- S_+) + \frac{1}{2}\hbar\sum_{j,\nu}(S_+ A_{-\nu} I_\nu^j + S_- A_{+\nu} I_\nu^j). \tag{B.3}$$

B.1 Secular Part—Energy Shifts

For ^{13}C spins beyond the first few shells, the hyperfine interaction is purely of dipolar form, and is given by

$$H_{\text{int}} = \sum_j \frac{\hbar^2\mu_e\mu_n}{r_j^3}\left(\vec{S}\cdot\vec{I}^j - 3\frac{(\vec{S}\cdot\vec{r}_j)(\vec{I}^j\cdot\vec{r}_j)}{r_j^2}\right), \tag{B.4}$$

Here, $\vec{I} = (I_x, I_y, I_z)$ and the distance between the NV and nuclear spin is $\vec{r_j} = r_j(\cos\phi\,\sin\theta, \sin\phi\,\sin\theta, \cos\theta)$.

Due to the enormous zero-field splitting ($\Delta/2\pi = 2.87$ GHz), we can think of this dipole–dipole interaction as a perturbation. The $S_{x,y}$ terms lead to electronic spin flips, and are highly suppressed due to ΔS_z^2 term. The energy mismatch between the electronic and nuclear spins ensures there is no flip-flop interaction as well. The dipole–dipole interaction for a single nuclear spin can thus be simplified to

$$H_{\text{int,j}} = \frac{\hbar^2\mu_n\mu_e}{r_j^3}\left(S_z I_z^j - 3S_z\cos\theta\left\{(I_x^j\cos\phi + I_y^j\sin\phi)\sin\theta + I_z^j\cos\theta\right\}\right). \tag{B.5}$$

Using $I_x = 1/2(I_+ + I_-)$ and $I_y = i/2(I_- - I_+)$, the above expression simplifies to

$$H_{\text{int,j}} = \frac{\hbar^2\mu_n\mu_e}{r_j^3}\left(S_z I_z^j(1 - 3\cos^2\theta) - \frac{3}{2}S_z\cos\theta\,\sin\theta(I_+^j e^{-i\phi} + I_-^j e^{i\phi})\right). \tag{B.6}$$

Thus, the hyperfine interaction leads to energy splittings in the NV center based on I_z and nuclear spin flips. The nuclear spin flips are suppressed if the nuclear Zeeman splitting is higher than the hyperfine interaction strength, i.e., $\hbar\mu_n B_z \gg \hbar^2\mu_n\mu_e/r_j^3$. This relation is valid for large magnetic fields, or large distance between the NV and nuclear spins. As an order of magnitude estimate, for B_z of around 1 Gauss, this relation is satisfied for distances greater than 1.4 nm. For a diamond sample with natural abundance of ^{13}C, the average $r_j \approx 1$ nm. Thus, this term cannot be ignored at first glance, and a lower concentration of ^{13}C sample might be preferable for this study. In the $|B\rangle,|D\rangle,|0\rangle$ basis, $S_z = |B\rangle\langle D| + |D\rangle\langle B|$ leading to flip-flop transitions between electronic and nuclear spin states via the term

$$H'_{\text{int},j} = \hbar\delta_z^j(|B\rangle\langle D| + |D\rangle\langle B|)(I_+^j\, e^{-i\phi} + I_-^j\, e^{i\phi}) \tag{B.7}$$

where δ_z takes into account the difference between hyperfine and Zeeman energy. Around $\delta = 0$, i.e., in the CPT dip, this leads to very slow transitions. For higher δ, these transitions are highly suppressed due to the mismatch in the nuclear and electronic spin energy difference. Furthermore, for higher δ, the probability of spin flips due to this mechanism is further suppressed due to the fact that the electronic spin is most likely in $|0\rangle$ state due to optical pumping, where there is no hyperfine interaction. Thus, in a simple treatment of bath dynamics, we ignore this nuclear spin flip mechanism.

These conditions are generally valid in the ^{13}C spin bath of an NV center, particularly close to the edge of the Overhauser distribution, where the external magnetic field is higher, and there is lower density of nuclear spin configurations. Thus we expect CPT based cooling to work most effectively in this region. For the purpose of this work, we assume that the hyperfine interaction is given by

$$H_{\text{int,j}} = \sum_j \frac{\hbar^2\mu_n\mu_e}{r_j^3} S_z I_z^j (1 - 3\cos^2\theta_j) = \sum_j \hbar A_{zz}^j S_z I_z^j. \tag{B.8}$$

It is clear from Eq. (B.8) that to leading order, the electronic spin experiences a static magnetic field of order $\sum_j A_{zz}^j/\mu_e$ as a result of interaction with the nuclear spin bath. Due to the possibility of being in various nuclear spin configurations, and hence different $\sum_j I_z^j$, the hyperfine

interaction leads to broadening of the $|\pm 1\rangle$ manifolds. We consider a more general expression for hyperfine interaction in order to calculate the correction to this treatment.

B.2 Nonsecular Part—Nuclear Bath Interactions

Using nondegenerate perturbation theory, and taking terms up to second order, the energy of the *i*-th eigenstate becomes (Yao and Shi, 2000)

$$E_i = E_i^{(0)} + \langle \phi_i | V | \phi_i \rangle + \langle \phi_i | V \hat{Q} \left(\sum_{k \neq i} \frac{|\phi_k\rangle\langle\phi_k|}{E_i^{(0)} - E_k^{(0)}} \right) \hat{Q} V | \phi_i \rangle, \tag{B.9}$$

where $|\phi_i\rangle$ are the unperturbed eigenstates, here $|0,\pm 1\rangle$, and $\hat{Q} = 1 - \hat{P}$, where $\hat{P} = |\phi_i\rangle\langle\phi_i|$ is the spin projection operator. For the NV, we get

$$E_0 = \frac{\langle 0|V|-1\rangle\langle -1|V|0\rangle}{E_0^{(0)} - E_{-1}^{(0)}} + \frac{\langle 0|V|1\rangle\langle 1|V|0\rangle}{E_0^{(0)} - E_1^{(0)}}, \tag{B.10}$$

$$E_{\pm 1} = E_{\pm 1}^{(0)} + \frac{\langle \pm 1|V|0\rangle\langle 0|V|\pm 1\rangle}{E_{\pm 1}^{(0)} - E_0^{(0)}}. \tag{B.11}$$

We use $E_0^{(0)} - E_{\pm 1}^{(0)} = -\hbar\Delta \mp \hbar\mu_e B_z \mp \sum_{j,\nu} A_{z\nu}^j I_\nu^j$ and $\langle 0|V|\pm 1\rangle = (\hbar/2)(\mu_e B_\pm + \sum_j \vec{A}_\pm^j . \vec{I}^j)$ and a bit of Pauli matrices identities($\vec{I} = (1/2)\,\vec{\sigma}$) and algebra to derive the second order corrections to the electronic energy levels. In the limit $\Delta \gg B, A_{z\nu}^j$, it simplifies to

$$E_{m_s}^{(2)} = \hbar \frac{(3m_s^2 - 2)}{4\Delta} \hat{M} - \hbar \frac{m_s}{4\Delta} \hat{N} \tag{B.12}$$

where

$$\hat{M} = \mu_e (B_x^2 + B_y^2) + \mathbf{A_-^j} . \mathbf{A_+^j} + \sum_j \mu_e (B_+ \mathbf{A_-^j} . \mathbf{I^j} + B_- \mathbf{A_+^j} . \mathbf{I^j}) + \sum_{j \neq k} (\mathbf{A_-^j} . \mathbf{I^j})(\mathbf{A_+^k} . \mathbf{I^k}), \tag{B.13}$$

$$\hat{N} = i \sum_j \mathbf{I^j} . (\mathbf{A_+^j} \times \mathbf{A_-^j}). \tag{B.14}$$

We can expand the second order correction and write it as

$$
\begin{aligned}
E^{(2)}_{m_s} = \; & \hbar\frac{(3m_s^2-2)}{4\Delta}(\mu_e(B_x^2+B_y^2)+\mathbf{A^j}_{-}\mathbf{A^j}_{+}) \\
& \hbar\frac{(3m_s^2-2)}{4\Delta}\sum_j \mu_e(B_+\mathbf{A^j}_{-}.\mathbf{I^j}+B_-\mathbf{A^j}_{+}.\mathbf{I^j}) - \hbar\frac{m_s}{4\Delta}i\sum_j \mathbf{I^j}.(\mathbf{A^j}_{+}\times\mathbf{A^j}_{-}) \\
& \hbar\frac{(3m_s^2-2)}{4\Delta}\sum_{j\neq k}(\mathbf{A^j}_{-}.\mathbf{I^j})(\mathbf{A^k}_{+}.\mathbf{I^k}),
\end{aligned}
\tag{B.15}
$$

where the first line of Eq. (B.15) gives a constant shift, while the second line acts as a modified gyromagnetic ratio, or nuclear spins in a fictitious magnetic field, and the third term leads to spin–spin interactions that are mediated by the hyperfine interaction of the two nuclear spins with the central spin. In general, these terms lead to change in nuclear spin configuration, and are present for all electronic states. However, due to the large hyperfine energy associated with nuclear spin flips when the NV is in state $|\pm 1\rangle$, this spin diffusion process is also suppressed. Thus, the diffusion model that leads to Lévy statistics will still be applicable in this case.

As an order of magnitude estimate, we evaluate the relative strength of interactions for the case of a single ^{13}C spin 1 nm away from the NV center, in an external B-field of 1 Gauss. Ignoring the angular dependence, the hyperfine interaction $A^j \sim 10$ kHz, and $\mu_e B \sim 1$ MHz, while $\Delta/2\pi = 2.87$ GHz. This gives us spin bath interaction strengths of $BA^j/\Delta \sim 10$ Hz, and $(A^j)^2/\Delta \sim 0.1$ Hz. Considering the nuclear Zeeman energy for the same B-field is ~ 1 kHz, spin flips as a result of hyperfine interaction will be suppressed, since they do not conserve energy. The hyperfine mediated flip-flop interaction is not suppressed due to this interaction. However, we have assumed that it is smaller than the dipole–dipole interaction between nuclei, i.e., $(A^j)^2/\Delta < D_{ij}$. If this last condition is not satisfied, the suppressed nuclear flip-flop rate $R_{n,D}$ will be given by this process, and not suppressed nuclear dipole–dipole interaction.

While these estimates may be satisfied in a naturally occurring concentration of ^{13}C, all these conditions are more likely to be satisfied in more sparse spin ensembles. However, we can have faster nuclear bath dynamics for higher concentration samples that makes measuring and modifying them easier. Since these are random distributions, care must be taken to ensure that there are no proximal nuclear spins in the vicinity of the NV center of interest in order to couple to a large number of spins similarly.

APPENDIX C. SIMULATING A REALISTIC ^{13}C SPIN BATH

In the following, we simulate the random ^{13}C nuclear spin bath around an NV center to estimate the distribution of hyperfine and nuclear bath interactions. These simulations are then used to discuss the effectiveness of nuclear spin cooling and emergence of Lévy statistics in nuclear diffusion.

We simulate a diamond lattice with an NV at the origin and a percentage of carbon atoms forming the lattice being ^{13}C ($I=1/2$) instead of ^{12}C ($I=0$). Due to the nonzero nuclear spin, they form an interacting spin bath surrounding the NV center. Such a system-bath interaction can be modeled as central spin system (Prokof'ev and Stamp, 2000). We only discuss the T_2 type relaxation of the bath (flip-flop processes), and its effect on the central spin, which in our case is the NV center. We evaluate the distribution of hyperfine and nuclear spin–spin interactions, identifying the physical mechanisms, and timescales for various spin diffusion processes for various concentrations of ^{13}C in diamond.

We then investigate the suppression of this relaxation if the NV is optically pumped into a dark state of $m_s=|\pm 1\rangle$ energy levels. This suppression is due to the hyperfine energy cost associated with spin-bath diffusion when the NV is not in $m_s=|0\rangle$ state. We discern the nuclear bath dynamics that leads to escape from the electronic dark state for various concentrations of the nuclear spins. Furthermore, we identify regions where such CPT based cooling is effective, and if the nuclear spin diffusion exhibits Lévy flights.

C.1 Concentration Study

We simulate three different spin baths, with varying concentration of ^{13}C spins: 11% (corresponding to enriched ^{13}C sample) or 1.1% (natural abundance ^{13}C sample), and 0.1% (sparse ^{13}C sample). In order to do a quantitative analysis of the bath interactions, we start with defining three frequencies: A_i characterizes the hyperfine interaction between an NV and i-th ^{13}C spin, D_{ij} estimates the nuclear dipole–dipole interaction between a pair of nuclear spins r_{ij} apart, and AD_{ij} estimates the hyperfine interaction induced spin–spin interaction between a pair of nuclear spins with off-axis hyperfine interaction strengths A_i and A_j, as given in Maze (2010). The hyperfine interaction includes both the dipole–dipole and contact interaction. The distance dependence of the hyperfine interaction for proximal spins is taken from previous measurements (Smeltzer et al., 2011). Since the bath is not polarized, the angular dependence of dipolar

interaction is taken into account by randomly selecting a polar angle between the spins. The bath interactions are given by

$$D_{ij} = \frac{\hbar}{4\pi}\frac{\mu_0}{4\pi}\frac{\hbar\mu_n^2}{r_{ij}^3}, \tag{C.1}$$

$$AD_{ij} = \frac{\hbar}{4\pi}\frac{A_i A_j}{\Delta}, \tag{C.2}$$

where for simplicity, we have ignored the angular dependence of the dipolar interaction, thus estimating the upper limit of various interactions. The largest value of D_{ij} is 1.03 kHz, corresponding to ^{13}C spins on adjacent lattice sites. The next highest D_{ij} is 237 Hz, corresponding to ^{13}C spins being at the next closest neighboring lattice sites. Due to the large Δ zero field splitting, AD_{ij} is only substantial for nuclear spin pairs close to the NV center, since they have large hyperfine interaction. In these cases, due to the large Fermi contact interaction component, we can ignore the angular dependence. For the closest ^{13}C spin, the A_i terms are around 2 kHz, thus they are the dominant spin–spin interactions for proximal nuclear spins. However, due to large zero-field splitting Δ, hyperfine interaction mediated nuclear interactions can be ignored for far-away spins.

For each spin bath concentration, we do a quantitative analysis of hyperfine and bath interactions, identifying the dominant dephasing mechanism for the bath spins. To get representative statistical samples, we simulate the interaction of around 700 ^{13}C spins with the NV center. It should be noted that in principle, the NV is coupled to an almost infinite spin bath of ^{13}C atoms[4]. Due to the weak hyperfine interaction of the NV with distant spins, these spins are not affected by the NV and vice-verse. However, the entire spin bath interacts with each other, forming the loss channel that ultimately limits the effectiveness of this, and every other nuclear cooling and dynamic polarization schemes.

C.1.1 Enriched ^{13}C Bath

Figure A.1 discusses the distribution of various interactions for an NV coupled to randomly positioned spins in an enriched ^{13}C bath with a 11% abundance. The abundance of ^{13}C spins enhances the proximal spin effects. The average interaction strength frequencies for this random bath are $\langle A_j \rangle = 145$ kHz, $\langle D_{ij} \rangle = 2.9$ Hz, $\langle AD_{ij} \rangle = 3.2$ Hz.

[4] Almost, since a diamond sample has a finite size.

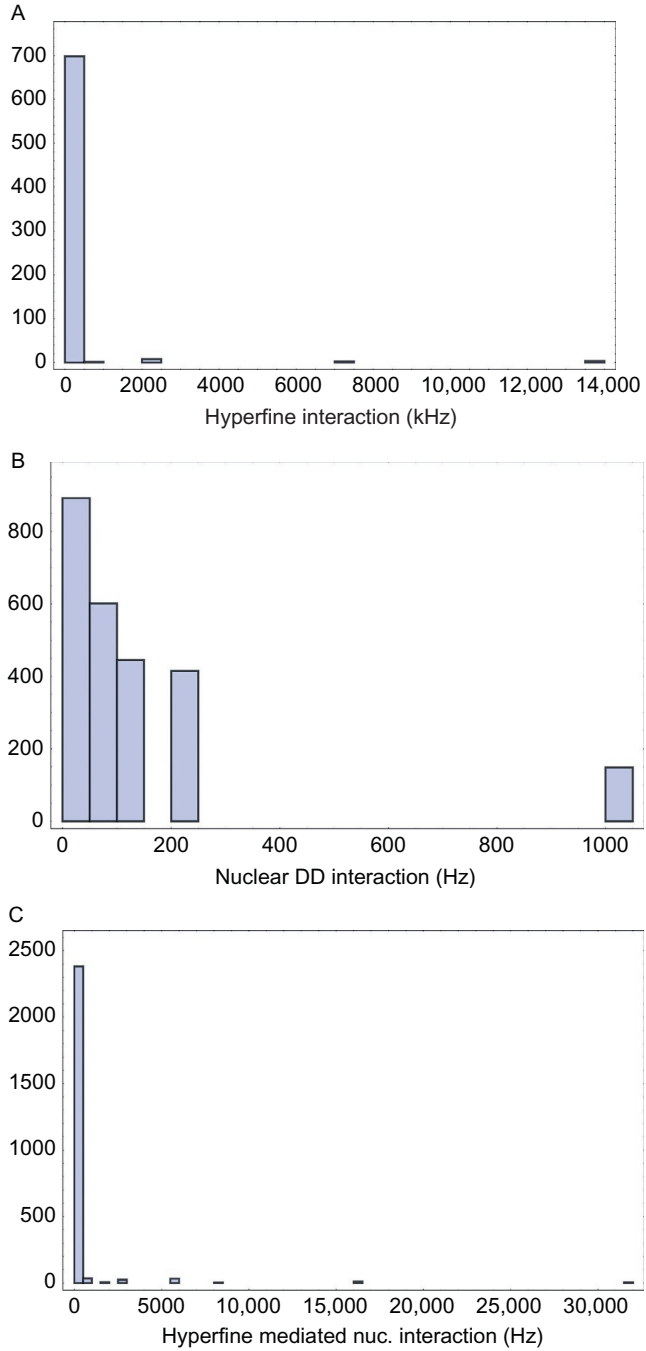

Figure A.1 Details of the proximal ^{13}C spin bath, when 11% of the diamond lattice is made of ^{13}C atoms. (a) Distribution of the hyperfine interactions A_i between NV center and a randomly located ^{13}C spin. (b) Distribution of the 2500 strongest dipole–dipole interactions D_{ij} between a pair of randomly located ^{13}C nuclei in a diamond lattice. (c) Distribution of the 2500 strongest NV mediated interactions between a pair of ^{13}C spins.

On first glance, it seems insignificant to consider nuclear spin–spin interaction induced flip-flops as the fastest nuclear bath dynamics (while ignoring Zeeman and hyperfine interaction mediated spin-flip mechanisms). However, in the presence of a magnetic field, such spin-flips are suppressed to conserve Zeeman energy. Furthermore, a significant fraction of spin pairs have much higher interaction strengths than the average, as shown in Fig. A.1b and c. These primarily include nuclear spins closest to the NV, thus causing a significant change in the Overhauser field by changing nuclear configuration. The distributions in Fig. A.1b and c also indicate that the primary source of nuclear dynamics is the NV induced flip-flops.

A stronger coupling to NV leads to fast nuclear bath dynamics in $|0\rangle$ state. A large hyperfine interaction energy shift leads to high suppression of nuclear dynamics in the electronic dark state. Both these effects combined lead to a strong freezing of the nuclear spin bath when the NV is in the optically dark state. However, there are several nuclear spin pairs that interact with each other more strongly than their interaction with the NV. Flip-flop interactions between such pairs leads to fast escape from the optical dark state. We shall study the competition between these interactions in more detail in the next section.

C.1.2 Natural Abundance ^{13}C Bath

Figure A.2 discusses the distribution of various interactions for an NV coupled to randomly positioned ^{13}C spins as well, but with a 1.1% abundance—the natural abundance of ^{13}C in diamond. Contrary to Fig. A.1c, we notice a more continuous distribution of hyperfine interaction induced energy level splitting with average $\delta_{ij}/2\pi = 25$ kHz for the 10 closest spins, as shown in Fig. A.2c. The average interaction strength frequencies are $\langle A_j \rangle = 1.5$ kHz, $\langle D_{ij} \rangle = 0.4$ Hz, $\langle AD_{ij} \rangle = 0.3$ mHz. While all these spin–spin interaction strengths are very small, as was the case before, a significant fraction of spins have much higher interaction strengths than the average, as shown in Fig. A.2b. These spin pairs dominate the bath dynamics. Contrary to the situation for enriched ^{13}C bath, this distribution indicates that the primary source of nuclear dynamics is bath dipole–dipole interaction induced flip-flops. While this mechanism for nuclear spin diffusion seems to be the average case, since we have a random distribution of ^{13}C spins, there may be some proximal spins present. In that case, the mechanism for flip-flops would be due to hyperfine interaction.

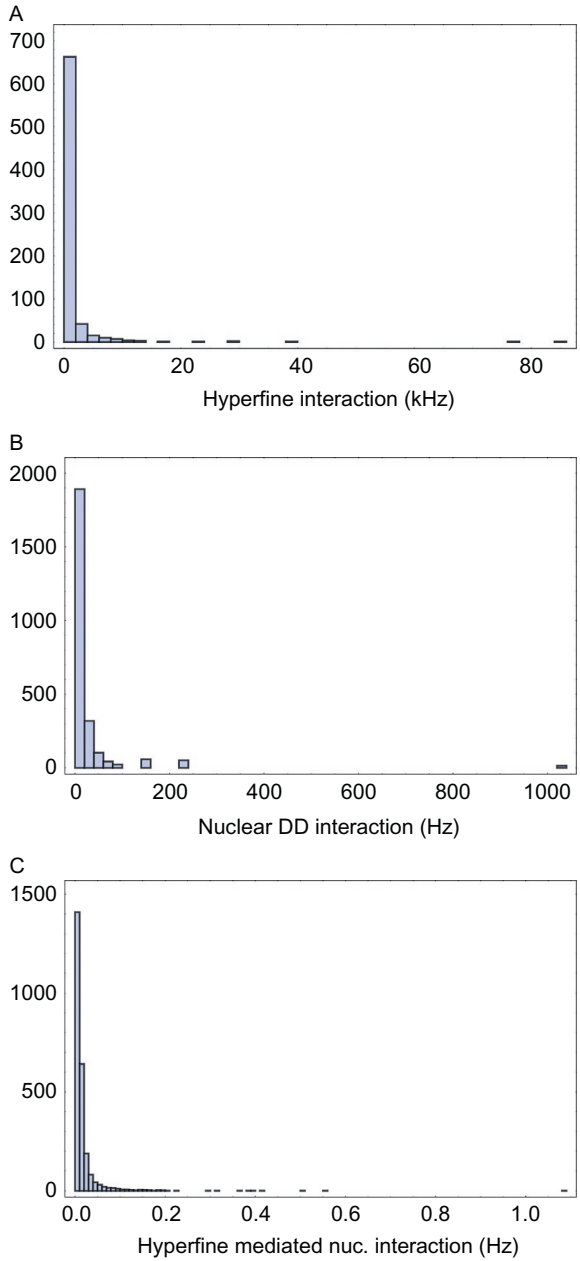

Figure A.2 Details of the ^{13}C spin bath, when 1.1% of the diamond lattice is made of ^{13}C atoms. (a) Distribution of the hyperfine interactions A_i between the NV center and a randomly located ^{13}C spin. (b) Distribution of the 2500 strongest dipole–dipole interactions D_{ij} between a pair of randomly located ^{13}C nuclei in a diamond lattice. (c) Distribution of the 2500 strongest NV mediated interactions between a pair of ^{13}C spins.

C.1.3 Sparse ^{13}C Bath

For completeness, we now move on to a sparse spin bath due to only 0.1% of carbon atoms being ^{13}C. As before, we estimate the interaction strengths for a bath of around 700 spins. The results are in Fig. A.3. A factor of two increase in distances compared to the previous case is as a result of increasing the volume of diamond by a factor of 10 to accommodate 700 spins. Due to the absence of proximal spins, the hyperfine interaction is very weak, as seen in Fig. A.3b. This results in a very small hyperfine mediated nuclear flip-flop interaction strength.

For this particular spin bath, $\langle A_j \rangle = 172$ Hz, $\langle D_{ij} \rangle = 0.057$ Hz, $\langle AD_{ij} \rangle = 4.82 \times 10^{-6}$ Hz. We notice a fragmented energy level structure, as shown in Fig. A.3c, which is similar to Fig. A.1, except for the orders of magnitude difference in the frequency difference between energy levels. The average $\delta_{ij}/2\pi$ is 20 Hz for the 10 closest spins. Due to the large difference between the hyperfine and nuclear dipole–dipole interaction, and a small number of nuclear spins interacting with the NV center, this spin bath is a good candidate to observe suppressed nuclear dynamics. The problem is that the timescales of the dynamics might too slow to be measured—particularly using optical techniques.

Given the timescales involved, a higher concentration of ^{13}C spins, forming a dense spin bath around the NV makes a more experimentally measurable system to study suppressed nuclear spin dynamics, and cooling of the spin bath. However, it may be possible to have a situation where a few spins are close to the NV, while the others are too far away to interact with the NV. This scenario is a special case of the central spin model, where we are indeed coupled to a finite (and manageable) spin bath, as opposed to an almost infinite one in other cases. Such a scenario can be used as a quantum simulator of driven out of equilibrium central spin system, particularly to address the implications of integrability in out-of-equilibrium quantum systems (Fioretto et al., 2014). Also, nano diamonds where different central spins are coupled to the same finite nuclear spin bath form another system to quantitatively analyze of the relation between integrability and decoherence (Erbe and Schliemann, 2010).

C.2 Nuclear Diffusion and Lévy Statistics

In the following, we analyze the efficiency of using CPT of the NV spin to suppress the nuclear bath dynamics. We identify the limitations of this spin cooling mechanism and discuss the prospects of Lévy flights in nuclear spin diffusion for realistic bath interactions.

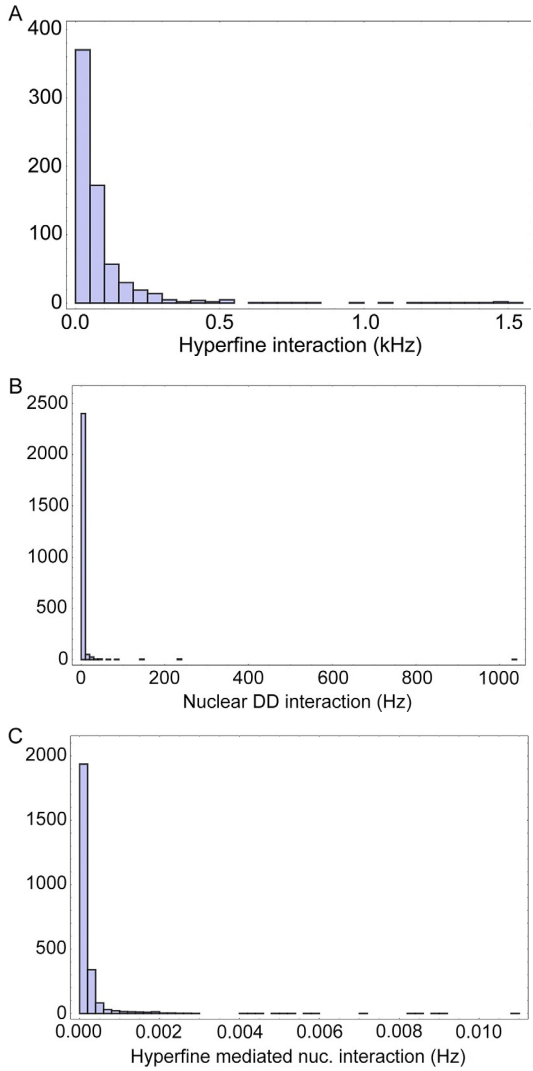

Figure A.3 Details of a sparse ^{13}C spin bath, when 0.1% of the diamond lattice is made of ^{13}C atoms. (a) Distribution of the hyperfine interactions A_i between NV center and a randomly located ^{13}C spin. (b) Distribution of the 2500 strongest dipole–dipole interactions D_{ij} between a pair of randomly located ^{13}C nuclei in a diamond lattice. (c) Distribution of the 2500 strongest NV mediated interactions between a pair of ^{13}C spins.

In order to establish notation, we summarize the suppression mechanism here. A pair of nuclear spins undergo flip-flop type interaction with frequency $\mathbf{\Omega}_{n0}$ in the absence of hyperfine interaction. As discussed earlier, this could be mediated by the NV itself, or due to dipole–dipole interaction

between nuclear spins themselves. We take Ω_{n0} to be the larger of D_{ij} or AD_{ij} calculated earlier for a specific spin pair.

In the presence of hyperfine interaction, there is a large energy cost associated with nuclear flip-flop transitions. The frequency of flip-flop gets reduced to $\Omega_{nD} = \Omega_{n0}^2 / \sqrt{\Omega_{n0}^2 + \delta_{ij}^2}$, where $\delta_{ij} = |A_i - A_j|$ is the difference of hyperfine energy (in frequency units) between the two nuclear configurations. Figure A.4 shows the distribution of Ω_{n0},Ω_{nD} for enriched, natural abundance and sparse ^{13}C bath samples. The details of nuclear spin cooling mechanism is discussed in detail in Section 2.5.

Since escape from the optically dark state is dominated by the fastest nuclear flip-flops, we identify three regions of interest, as highlighted in Fig. A.4. These form different parameter regimes of CPT based spin bath cooling. We discuss these in more detail in the following.

C.2.1 Region 1—Fast Decay, Low Suppression ($\delta_{ij} \ll R_{AB}$)

Region 1 indicates nearby (typically nearest neighbor) spin pairs undergoing fast flip-flops due to strong dipole–dipole interaction between them. This dynamics is not highly suppressed because the hyperfine energy difference between the two spin configurations is very small. *This is the prominent escape mechanism from the dark state*. Typically these are spins far away from the NV as well, so they do not effect the Overhauser field significantly. These far away, weakly interacting spins form the fundamental limit for this, and most other dynamic polarization schemes for the nuclear spin bath.

Dynamics of region 1 becomes dominant when we have a very sharp CPT dip where changes of a few kHz in δ leads to large population difference between $|D\rangle$ and $|0\rangle$ states. While this may not lead to good cooling, this may be used as a method to optically detect far away nuclear spins.

C.2.2 Region 2—Slow Decay, Large Suppression ($\delta_{ij} \gg R_{AB}$)

Region 2 indicates NV induced spin flips in the nearby nuclear spin pairs. This is predominant in enriched ^{13}C samples. Due to the large hyperfine energy difference between two spin configurations (typically larger than CPT width), this diffusion gets suppressed by orders of magnitude due to the formation of a dark state. While this may be the fastest diffusion rate into the dark state, this is not the fastest decay rate out of the dark state. However, if the NV was strongly coupled to very few spins, the nuclear bath dynamics would be determined by these optically suppressed rates, leading to very efficient freezing of the nuclear dynamics (as is the case for ^{14}N spin cooling).

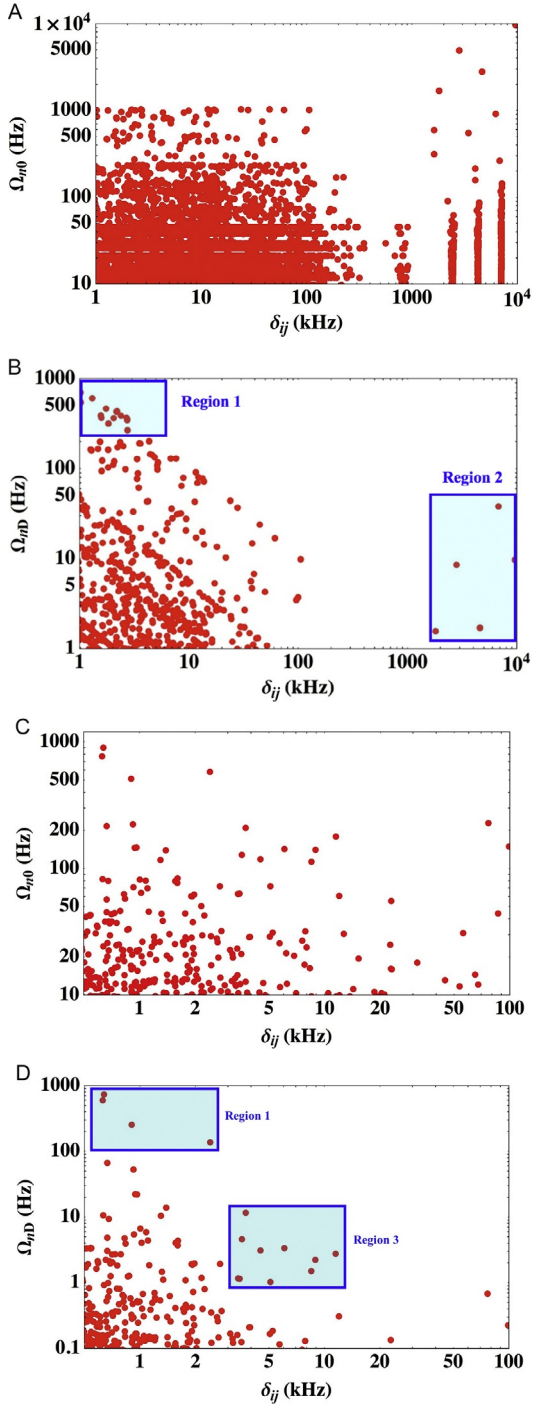
A
1×10^4
5000
1000
500
100
50
10
Ω_{n0} (Hz)
1
10
100
1000
10^4
δ_{ij} (kHz)
B
1000
500
100
50
10
5
1
Ω_{nD} (Hz)
Region 1
Region 2
1
10
100
1000
10^4
δ_{ij} (kHz)
C
1000
500
200
100
50
20
10
Ω_{n0} (Hz)
1
2
5
10
20
50
100
δ_{ij} (kHz)
D
1000
100
10
1
0.1
Ω_{nD} (Hz)
Region 1
Region 3
1
2
5
10
20
50
100
δ_{ij} (kHz)

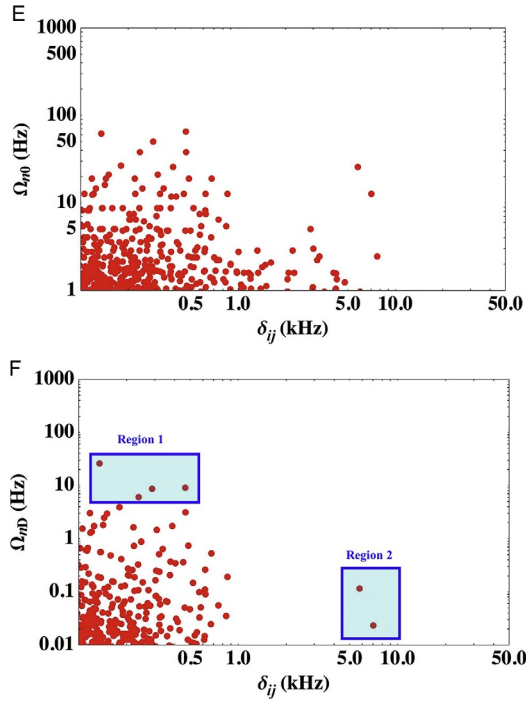

Figure A.4 Distribution of flip-flop transition frequencies for various ^{13}C spin baths, in the absence and presence of hyperfine interaction. (a) Distribution of transition frequencies in the absence of hyperfine interaction (Ω_{n0}), (b) suppressed diffusion rates due to dark state formation (Ω_{nD}) for an enriched ^{13}C bath, (c and d) for a natural abundance of ^{13}C atoms, and (e and f) for a sparse ^{13}C bath.

C.2.3 Region 3—Lévy Statistics Region ($\delta_{ij} < R_{AB}$)

Between these two extremes lies the region where the hyperfine energy difference is large enough to suppress nuclear dynamics in the dark state, but not larger than the width of the CPT dip. This gives us a large, *detuning dependent* nuclear diffusion rate that leads to power law suppression of nuclear dynamics. Such spin pairs are indicated in region 3.

Experimentally, this region can be accessed by using strong pumping lasers such that the CPT width is large. This leads to little change in population difference between $|D\rangle$ and $|0\rangle$ over a few kHz, where fast nuclear diffusion due to adjacent spin pairs occurs. While this fast diffusion is not suppressed, it also does not lead to escape from the optical dark state.

Provided we have large suppression of nuclear dynamics in the dark state (occurs when $\delta_{ij} \gg \Omega_{n0}$), but there are several nuclear configurations in the CPT region ($\delta_{ij} < R_{AB}$), we have a detuning dependent suppression of nuclear bath dynamics. If this suppression is well over an order of magnitude ($\Omega_{nD} \ll \Omega_{n0}$), we have a power law distribution function for jumps between adjacent configurations leading to Lévy statistics. For realistic ^{13}C baths considered in the previous section, it seems to be a valid assumption for a large number of spins close to the NV.

However, the condition $\delta_{ij} \gg \Omega_{n0}$ is not necessarily satisfied for all nuclear configurations—particularly the distant spins, as is visible in Fig. A.4. Furthermore, numerical simulations show that while a large suppression is essential for a power law distribution of jump times, the power itself depends on how close different δ states are. All else being the same, a fine integration of δ gives us a power closer to $-3/2$, while a coarse integration over δ states gives us higher power laws that may or may not lead to diverging moments. These contradicting conditions for suppression of nuclear dynamics and observation of 3/2 power law lead us to be cautiously optimistic about actual observation of Lévy statistics in nuclear spin dynamics.

However, there is definitely cooling of the spin bath since all the proximal spins are frozen when the NV is in the dark state, and their configuration change occurring at much longer timescales. It may be possible to observe a power law diffusion closer to the edge of the Overhauser field where there are fewer and well-separated energy levels.

For the purpose of nuclear diffusion estimates, we assume a natural abundance diamond sample. Based on our simulations, we have taken $D_{ij} = 230$ Hz, and $\delta_{ij} = 10$ kHz. For the low B-fields and natural abundance sample considered in this work, these numbers are justified. Based on realistic bath estimates, it is our opinion that while there are regimes to observe large nuclear spin cooling, to observe real-time dynamics of the interacting spin bath, and to see Lévy statistics in photon diffusion, the actual observation of a power law in the cooling of the nuclear spin bath showing Lévy flights in nuclear spin cooling over several decades might be challenging for experimentally accessible parameter regimes due to the slow nuclear spin dynamics involved.

REFERENCES

Abragam, A., 1983. Principles of Nuclear Magnetism. Oxford University Press.

Aspect, A., Arimondo, E., Kaiser, R., Vansteenkiste, N., Cohen-Tannoudji, C., 1988. Laser cooling below the one-photon recoil energy by velocity-selective coherent population trapping. Phys. Rev. Lett. 61 (7), 826–829. http://dx.doi.org/10.1103/PhysRevLett.61.826.

Aspect, A., Arimondo, E., Kaiser, R., Vansteenkiste, N., Cohen-Tannoudji, C., 1989. Laser cooling below the one-photon recoil energy by velocity-selective coherent population trapping: theoretical analysis. J. Opt. Soc. Am. B 6, 2112–2124.

Awschalom, D.D., Bassett, L.C., Dzurak, A.S., Hu, E.L., Petta, J.R., 2013. Quantum spintronics: engineering and manipulating atom-like spins in semiconductors. Science 339 (6124), 1174–1179.

Balasubramanian, G., Chan, I.Y., Kolesov, R., Al-Hmoud, M., Tisler, J., Shin, C., Kim, C., Wjcik, A., Hemmer, P.R., Krueger, A., Hanke, T., Leitenstorfer, A., Bratschitsch, R., Jelezko, F., Wrachtrup, J., 2008. Nanoscale imaging magnetometery with diamond spins under ambient conditions. Nature 455, 648–651.

Baranov, P.G., Bundakova, A.P., Soltamova, A.A., Orlinskii, S.B., Borovykh, I.V., Zondervan, R., Verberk, R., Schmidt, J., 2011. Silicon vacancy in SiC as a promising quantum system for single-defect and single-photon spectroscopy. Phys. Rev. B 83, 125203.

Bardou, F., Bouchaud, J.P., Aspect, A., Cohen-Tannoudji, C., 2002. Lévy Satistics and Laser Cooling. Cambridge University Press.

Batalov, A., Jacques, V., Kaiser, F., Siyushev, P., Neumann, P., Rogers, L.J., McMurtrie, R.L., Manson, N.B., Jelezko, F., Wrachtrup, J., 2009. Low temperature studies of the excited-state structure of negatively charged nitrogen-vacancy color centers in diamond. Phys. Rev. Lett. 102 (19), 195506. http://dx.doi.org/10.1103/PhysRevLett.102.195506.

Bernien, H., Hensen, B., Pfaff, W., Koolstra, G., Blok, M.S., Robledo, L., Taminiau, T.H., Markham, M., Twitchen, D.J., Childress, L., Hanson, R., 2013. Heralded entanglement between solid-state qubits separated by three metres. Nature 497, 8690.

Buckley, B.B., Fuchs, G.D., Bassett, L.C., Awschalom, D.D., 2010. Spin-light coherence for single-spin measurement and control in diamond. Science 330 (6008), 1212–1215. http://dx.doi.org/10.1126/science.1196436.

Budker, D., Romalis, M., 2007. Optical magnetometry. Nat. Phys. 3, 227–234.

Childress, L., Gurudev Dutt, M.V., Taylor, J.M., Zibrov, A.S., Jelezko, F., Wrachtrup, J., Hemmer, P.R., Lukin, M.D., 2006. Coherent dynamics of coupled electron and nuclear spin qubits in diamond. Science 314 (5797), 281–285. http://dx.doi.org/10.1126/science.1131871.

Childress, L., Walsworth, R., Lukin, M., 2014. Atom-like crystal defects: from quantum computers to biological sensors. Phys. Today 0031-9228.67 (10), 38–43. http://dx.doi.org/10.1063/PT.3.2549. URL, http://scitation.aip.org/content/aip/magazine/physicstoday/article/67/10/10.1063/PT.3.2549.

Chu, Y., Lukin, M.D., 2014. Quantum optics with nitrogen-vacancy centers in diamond. URL, http://arxiv.org/abs/1504.05990.

Cohen-Tannoudji, C., Dalibard, J., 1986. Single-atom laser spectroscopy: looking for dark periods in fluorescence light. Europhys. Lett. 1 (9), 441.

Dréau, A., Jamonneau, P., Gazzano, O., Kosen, S., Roch, J.F., Maze, J.R., Jacques, V., 2014. Probing the dynamics of a nuclear spin bath in diamond through time-resolved central spin magnetometry. Phys. Rev. Lett. 113, 137601.

Dutt, M.V.G., Childress, L., Jiang, L., Togan, E., Maze, J., et al., 2007. Quantum register based on individual electronic and nuclear spin qubits in diamond. Science 316, 1312.

Erbe, B., Schliemann, J., 2010. Different types of integrability and their relation to decoherence in central spin models. Phys. Rev. Lett. 105, 177602.

Fioretto, D., Caux, J.S., Gritsev, V., 2014. Exact out-of-equilibrium central spin dynamics from integrability. New J. Phys. 16 (4), 043024.

Fleischhauer, M., Imamoglu, A., Marangos, J.P., 2005. Electromagnetically induced transparency: optics in coherent media. Rev. Mod. Phys. 77, 633.

Fuchs, G.D., Dobrovitski, V.V., Hanson, R., Batra, A., Weis, C.D., Schenkel, T., Awschalom, D.D., 2008. Excited-state spectroscopy using single spin manipulation in

diamond. Phys. Rev. Lett. 101 (11), 117601. http://dx.doi.org/10.1103/PhysRevLett.101.117601.
Giedke, G., Taylor, J.M., D'Alessandro, D., Lukin, M.D., Imamoglu, A., 2006. Quantum measurement of a mesoscopic spin ensemble. Phys. Rev. A 74 (3), 032316. http://dx.doi.org/10.1103/PhysRevA.74.032316.
Hall, L.T., Cole, J.H., Hollenberg, L.C.L., 2014. Analytic solutions to the central-spin problem for nitrogen-vacancy centers in diamond. Phys. Rev. B 90, 075201.
Hanson, R., Gywat, O., Awschalom, D.D., 2006. Room-temperature manipulation and decoherence of a single spin in diamond. Phys. Rev. B 74, 161203(R).
Hennessy, K., Badolato, A., Winger, M., Gerace, D., Atatüre, M., Gulde, S., Fält, S., Hu, E.L., Imamoglu, A., 2007. Quantum nature of a strongly coupled single quantum dot-cavity system. Nature 445, 896–899.
Issler, M., Kessler, E.M., Giedke, G., Yelin, S., Cirac, I., Lukin, M.D., Imamoglu, A., 2010. Nuclear spin cooling using overhauser-field selective coherent population trapping. Phys. Rev. Lett. 105 (26), 267202. http://dx.doi.org/10.1103/PhysRevLett.105.267202.
Kucsko, G., Maurer, P.C., Yao, N.Y., Kubo, M., Noh, H.J., Lo, P.K., Park, H., Lukin, M.D., 2013. Nanometre-scale thermometry in a living cell. Nature 500, 54–58.
Maletinsky, P., Hong, S., Grinolds, M.S., Hausmann, B., Lukin, M.D., Walsworth, R.L., Loncar, M., Yacoby, A., 2012. A robust scanning diamond sensor for nanoscale imaging with single nitrogen-vacancy centres. Nat. Nanotechnol. 7, 320–324.
Manson, N.B., Harrison, J.P., Sellars, M.J., 2006. Nitrogen-vacancy center in diamond: model of the electronic structure and associated dynamics. Phys. Rev. B 74, 104303. http://dx.doi.org/10.1103/PhysRevB.74.104303.
Mantegna, R.N., Stanley, H.E., 1994. Stochastic process with ultraslow convergence to a Gaussian: the truncated Lévy flight. Phys. Rev. Lett. 73, 2946–2949.
Maze, J.R., 2010. Quantum manipulation of nitrogen-vacancy centers in diamond: from basic properties to applications. Ph.D. thesis, Harvard University, An optional note.
Maze, J.R., Stanwix, P.L., Hodges, J.S., Hong, S., Taylor, J.M., Cappellaro, P., Jiang, L., Dutt, M.V.G., Togan, E., Zibrov, A.S., Yacoby, A., Walsworth, R.L., Lukin, M.D., 2008. Nanoscale magnetic sensing with an individual electronic spin in diamond. Nature 455, 644–647.
Maze, J., Gali, A., Togan, E., Chu, Y., Trifonov, A., Kaxiras, E., Lukin, M., 2011. Properties of nitrogen-vacancy centers in diamond: the group theoretic approach. New J. Phys. 13, 025025.
Mizuochi, N., Neumann, P., Rempp, F., Beck, J., Jacques, V., Siyushev, P., Nakamura, K., Twitchen, D.J., Watanabe, H., Yamasaki, S., Jelezko, F., Wrachtrup, J., 2009. Coherence of single spins coupled to a nuclear spin bath of varying density. Phys. Rev. B 80, 041201.
Mølmer, K., Castin, Y., Dalibard, J., 1993. Monte Carlo wave-function method in quantum optics. J. Opt. Soc. Am. B 10, 524–538.
Neumann, P., Mizuochi, N., Rempp, F., Hemmer, P., Watanabe, H., Yamasaki, S., Jacques, V., Gaebel, T., Jelezko, F., Wrachtrup, J., 2008. Multipartite entanglement among single spins in diamond. Science 320 (5881), 1326–1329.
Neumann, P., Beck, J., Steiner, M., Rempp, F., Fedder, H., Hemmer, P.R., Wrachtrup, J., Jelezko, F., 2010. Single-shot readout of a single nuclear spin. Science 329, 542.
Ni, K.K., Ospelkaus, S., de Miranda, M.H.G., Pe'er, A., Neyenhuis, B., Zirbel, J.J., Kotochigova, S., Julienne, P.S., Jin, D.S., Ye, J., 2008. A high phase-space-density gas of polar molecules. Science 322 (5899), 231–235. http://dx.doi.org/10.1126/science.1163861.
Prokof'ev, N., Stamp, P., 2000. Theory of the spin bath. Rep. Prog. Phys. 63 (4), 669.

Robledo, L., Bernien, H., van Weperen, I., Hanson, R., 2010. Control and coherence of the optical transition of single nitrogen vacancy centers in diamond. Phys. Rev. Lett. 105, 177403. http://dx.doi.org/10.1103/PhysRevLett.105.177403.

Roos, C.F., Leibfried, D., Mundt, A., Schmidt-Kaler, F., Eschner, J., Blatt, R., 2000. Experimental demonstration of ground state laser cooling with electromagnetically induced transparency. Phys. Rev. Lett. 85, 5547.

Sage, D.L., Arai, K., Glenn, D.R., DeVience, S.J., Pham, L.M., Rahn-Lee, L., Lukin, M.D., Yacoby, A., Komeili, A., Walsworth, R.L., 2013. Optical magnetic imaging of living cells. Nature 496, 486–489.

Santori, C., Tamarat, P., Neumann, P., Wrachtrup, J., Fattal, D., Beausoleil, R.G., Rabeau, J., Olivero, P., Greentree, A.D., Prawer, S., Jelezko, F., Hemmer, P., 2006. Coherent population trapping of single spins in diamond under optical excitation. Phys. Rev. Lett. 97 (24), 247401. http://dx.doi.org/10.1103/PhysRevLett.97.247401.

Scully, M.O., Fleischhauer, M., 1992. High-sensitivity magnetometer based on index-enhanced media. Phys. Rev. Lett. 69 (9), 1360–1363. http://dx.doi.org/10.1103/PhysRevLett.69.1360.

Scully, M.O., Zubairy, M.S., 1997. Quantum Optics. Cambridge University Press.

Smeltzer, B., Childress, L., Gali, A., 2011. 13C hyperfine interactions in the nitrogen-vacancy centre in diamond. New J. Phys. 13 (2), 025021.

Stepanenko, D., Burkard, G., Giedke, G., Imamoglu, A., 2006. Enhancement of electron spin coherence by optical preparation of nuclear spins. Phys. Rev. Lett. 96 (13), 136401. http://dx.doi.org/10.1103/PhysRevLett.96.136401.

Togan, E., Chu, Y., Trifonov, A.S., Jiang, L., Maze, J., Childress, L., Dutt, M.V.G., Sørensen, A.S., Hemmer, P.R., Zibrov, A.S., Lukin, M.D., 2010. Quantum entanglement between an optical photon and a solid-state spin qubit. Nature (London) 0028-0836. 466 (7307), 730–734. http://dx.doi.org/10.1038/nature09256.

Togan, E., Chu, Y., Imamoglu, A., Lukin, M.D., 2011. Laser cooling and real-time measurement of the nuclear spin environment of a solid-state qubit. Nature 478 (7370), 497–501.

Vanier, J., 2005. Atomic clocks based on coherent population trapping: a review. Appl. Phys. B: Lasers Opt. 0946-2171. 81, 421–442.

Wang, P., Du, J., Yang, W., 2014. Quantum theory of nuclear spin dynamics in diamond nitrogen-vacancy center, ArXiv:1409.1482v1.

Weber, J.R., Koehl, W.F., Varley, J.B., Janotti, A., Buckley, B.B., de Walle, C.G.V., Awschalom, D.D., 2010. Quantum computing with defects. Proc. Natl. Acad. Sci. 107 (19), 8513–8518.

Wrachtrup, J., Jelezko, F., 2006. Processing quantum information in diamond. J. Phys.: Condens. Matter 18 (21), S807.

Xu, X., Yao, W., Sun, B., Steel, D.G., Bracker, A.S., Gammon, D., Sham, L.J., 2009. Optically controlled locking of the nuclear field via coherent dark-state spectroscopy. Nature 459, 1105–1109.

Yao, D., Shi, J., 2000. Projection operator approach to time-independent perturbation theory in quantum mechanics. Am. J. Phys. 68 (3).

Zhao, N., Ho, S.W., Liu, R.B., 2012. Decoherence and dynamical decoupling control of nitrogen vacancy center electron spins in nuclear spin baths. Phys. Rev. B 85, 115303.

Zoller, P., Marte, M., Walls, D.F., 1987. Quantum jumps in atomic systems. Phys. Rev. A 35, 198–207.